AGU ADVANCING EARTH AND SPACE SCIENCE

Earth and Space Science

RESEARCH ARTICLE
10.1029/2021EA001930

Spatio-Temporal Changes in Extreme Rainfall Events Over Different Indian River Basins

Pawan K. Chaubey[1], R. K. Mall[1], Rohit Jaiswal[1], and Swagata Payra[2]

[1]DST-Mahamana Centre of Excellence in Climate Change Research, Institute of Environment and Sustainable Development, Banaras Hindu University, Varanasi, India, [2]Department of Physics, Birla Institute of Technology Mesra, Jaipur Campus, Jaipur, India

Key Points:

- High-resolution gridded data sets used for the assessment of the rainfall extremes over the Indian River Basins (IRBs)
- A western shift in a significantly increasing trend of extreme rainfall events was observed over the western part of the IRBs in the last four decades
- West and North-east flowing river basins were found to be highly flood-prone regions resulting in vulnerable hazards

Supporting Information:

Supporting Information may be found in the online version of this article.

Correspondence to:

R. K. Mall,
rkmall@bhu.ac.in

Citation:

Chaubey, P. K., Mall, R. K., Jaiswal, R., & Payra, S. (2022). Spatio-temporal changes in extreme rainfall events over different Indian river basins. *Earth and Space Science*, *9*, e2021EA001930. https://doi.org/10.1029/2021EA001930

Received 24 JUL 2021
Accepted 9 FEB 2022

Author Contributions:

Conceptualization: R. K. Mall
Data curation: Pawan K. Chaubey, Rohit Jaiswal
Formal analysis: Pawan K. Chaubey
Funding acquisition: R. K. Mall
Investigation: Pawan K. Chaubey, R. K. Mall
Methodology: Pawan K. Chaubey, R. K. Mall
Project Administration: R. K. Mall

Abstract During recent decades, India experienced more frequent and severe floods due to increasing extreme rainfall events over different Indian River Basins (IRBs). The present study uses Generalized Extreme Value distribution, Expert Team on Climate Change and Detection Indices, and Standardized Precipitation Index to examine the trend in extreme rainfall events over the IRBs using long-term observed high-resolution gridded rainfall data (1901-2019) obtained from India Meteorological Department. The analysis depicts a marked shifting trend in extreme rainfall events from northeastern Indian river basins toward the western Indian river basins during the recent decades of 1981-2019. The spatial variations in the annual maximum rainfall for the 10-, 30-, and 100-year return levels show statistically significant increasing trends over the IRBs. The observed decadal changes of rainfall during wet and dry conditions showed the shifting and increasing (15%–58.74%) pattern in extreme rainfall events during the last decades of the 20th and current twenty first century over the west-flowing river basins. This research highlights the significant increasing trend in extreme rainfall events, which may pose a grave risk to agriculture, human life, and infrastructure, predominantly on the vulnerable sections of the society.

1. Introduction

In the wake of recent global warming, an increase in extreme weather events such as extreme rainfall is observed globally, which has a severe impact on natural and man-made ecosystems (IPCC, 2014; Libertino et al., 2019; Papalexiou & Montanari, 2019). In recent decades, it was observed that around 20 to 80 million of the global population is affected by floods every year, whereas India has observed the most significant loss to life and property due to extreme rainfall events (EM-DAT, 2019). More than 279 reported flood events in India from 1953 to 2018, affecting about 2.167 billion population, killing more than one lakh people, and causing damage to more than 258 Mha crop area (CWC, 2019). About 75% of the Indian districts are vulnerable to extreme weather events, whereas 55 districts experienced floods every year between 2005 and 2019. However, the frequency of flood events increased eight times in the last 50-year (Mohanty, 2020).

Prior studies have reported that under a warming climate, extreme rainfall events have significantly increased during the post-urbanization era, resulting in the increasing risk of flood over the river basins (Ali et al., 2019; Bisht et al., 2018; Hodgkins et al., 2019; Lu et al., 2019). Krishnamurthy et al. (2009) reported a significant increasing trend in rainfall extremes over India. While an increasing trend in the spatial variability of extreme rainfall was noticed by applying space-time statistical regression analysis at different return levels. Ghosh et al., 2009 reported that the Generalized Extreme Value (GEV) theory displayed no significant spatial trends on annual maximum rainfall over India (Dash et al., 2009). Roxy et al. (2017) found that central India, where 60% of the agriculture is rainfed, experienced a threefold rise in extreme rainfall events after the mid-twentieth century (1950–2015). Agriculture contributes around 17% to India's GDP, and it's very much dependent on rainfall. Extreme rainfall events over India are linked to global teleconnections such as El Niño–Southern Oscillation (ENSO) and Pacific Decadal Oscillation (PDO). These are responsible for interannual rainfall variability over different Indian River Basins (IRBs; Bishop et al. [2019]; Carvalho [2020]; Mall et al. [2006]; Raj et al. [2020]; Shah & Mishra [2021]). Cai et al. (2014) reported that the increased frequency of the extreme Indian Ocean Dipole (IOD) events due to global warming has led to the more frequent occurrence of devastating extreme precipitation events over regions affected by pacific IOP events, which include India as well. While extreme rainfall events are reported to have risen, a significant decreasing trend in low to moderate rainy days has been

Resources: R. K. Mall
Software: Pawan K. Chaubey, Rohit Jaiswal
Supervision: R. K. Mall
Validation: Pawan K. Chaubey, Rohit Jaiswal
Visualization: Pawan K. Chaubey, Rohit Jaiswal
Writing – original draft: Pawan K. Chaubey
Writing – review & editing: R. K. Mall, Swagata Payra

observed during the end of the twentieth century (Dash et al., 2009). This increase in extreme rainfall events and decrease in low to moderate rainy days give rise to flood and drought conditions over India.

India's large population depends on the summer monsoon rainfall for agriculture (Turner & Annamalai, 2012), which is affected by extreme rainfall over the IRBs (Devanand et al., 2019). Floods due to extreme rainfall in different Indian river basins alone amounted to 10% of global economic losses (Mall et al., 2019; Roxy et al., 2017). The increasing pattern of extreme rainfall over the IRBs results in flash floods, landslides, crop damage which severely impacts the society as well as the economy of the area (Deshpande et al., 2016; Ghosh et al., 2009, 2012; Goswami et al., 2006; Krishnamurthy et al., 2009; Rajeevan et al., 2006, 2008; Suman & Maity, 2020). GEV framework has been widely used to study the behavior of extreme precipitation events responsible for severe hydro-meteorological disasters in many studies over different regions (Charn et al., 2020; Khan et al., 2007; Martins & Stedinger, 2000; Tabari, 2020; Van De Vyver, 2012). The GEV distribution is based on the extreme value theory (EVT) and infers the tail behavior of the rainfall series at different return levels, such as at 100-year return levels (or 1% probability storms), based on well-grounded statistical theory (Ghosh et al., 2012; Kunkel et al., 2003; Sanderson et al., 2019). Many researchers have also adopted Standardized precipitation indices (SPI) for identifying the wet and dry period for 12-month's time window with monthly rainfall as an input that indicates the long-term wet period over any study area (Hänsel et al., 2016; Trenberth et al., 2014). SPI was propounded by McKee (1993), as an essential tool for monitoring the rainfall variation in an aspect of highly wet condition situations over a region. Most of the previous climate change impact studies adopted the multitude of indices recommended by the Expert Team on Climate Change Detection and Indices (ETCCDI) for climate extreme impact assessment (Ayugi et al., 2020; Ogega et al., 2020; Santos et al., 2019; Tegegne & Melesse, 2020; Tong et al., 2019; Zhang et al., 2011). The ETCCDI indices are significant to detect a trend in the projected climate extremes, calculated based on the fixed threshold, duration, absolute, and percentile of climate variables using the standard algorithm provided by ETCCDI (Zhang et al., 2011). Previous researchers have analyzed rainfall extremes using ETCCDI indices based on the daily rainfall frequency (Herold et al., 2017; Tegegne et al., 2021).

Previous research focusing on the observed rainfall extremes over the IRBs during the twentieth century and recent decades of the twenty first century shows scarce evidence on shifting of the extreme rainfall events. However, despite several studies conducted in the past, a focused approach that considers the long-term changes in rainfall extremes over IRB was not undertaken. Moreover, the investigation of any shift in the spatio-temporal trend of extreme rainfall events over the IRBs that lacked in the previous studies is targeted in the current study.

Therefore, the present study aims to analyze the (a) Changes in rainfall extremes in a 40-year running period and (b) spatially shifting patterns of the extreme rainfall events over the IRBs during 1901-2019.

2. Material and Methods

2.1. Study Area and Data

The study area comprises 22 IRBs which lie between 8.4° and 37.6°N latitude and 68.7° to 97.25°E longitude (Figure 1) in India. According to Guhathakurta and Rajeevan (2008), based on the climatology of rainfall and temperature, the Indian region has been categorized as four different homogenous climatic regions which are North-West India (NW India), North-East India (NE India), Central India, and Peninsular India (Saha et al., 2017). This study divides the IRBs according to the homogenous climate regions as North-West India river basins (NW-IRBs), North-East India river basins (NE-IRBs), Central India river basins (CI-IRBs), and Peninsular India river basin (PI-IRBs). To estimate the extreme rainfall over the IRBs, we have used the long-term (1901-2019) high-resolution daily gridded rainfall data generated at 0.25° × 0.25° spatial resolution by IMD using 6,955 rain gauges across India (Pai et al., 2014, 2015). The 22 major IRBs have been extracted by using a Digital Evaluation Model (DEM) taken from Shuttle Radar Topography Mission (SRTM). It considers similar topography as boundary according to the Indian river basin atlas published by Water Resources Information System (WRIS; CWC [2018]; India-WRIS [2012]). This study used SRTM with 30-m resolution (1 arc-second global coverage). DEM is supposed to be more useful to extract the river watersheds than ASTER (Advanced Spaceborne Thermal Emission and Reflection Radiometer) because SRTM considers radar observations to get perfect topographic extent while ASTER uses stereo imagery and photogrammetric techniques. The name and details of the 22 major IRBs are listed and shown in Figure 1.

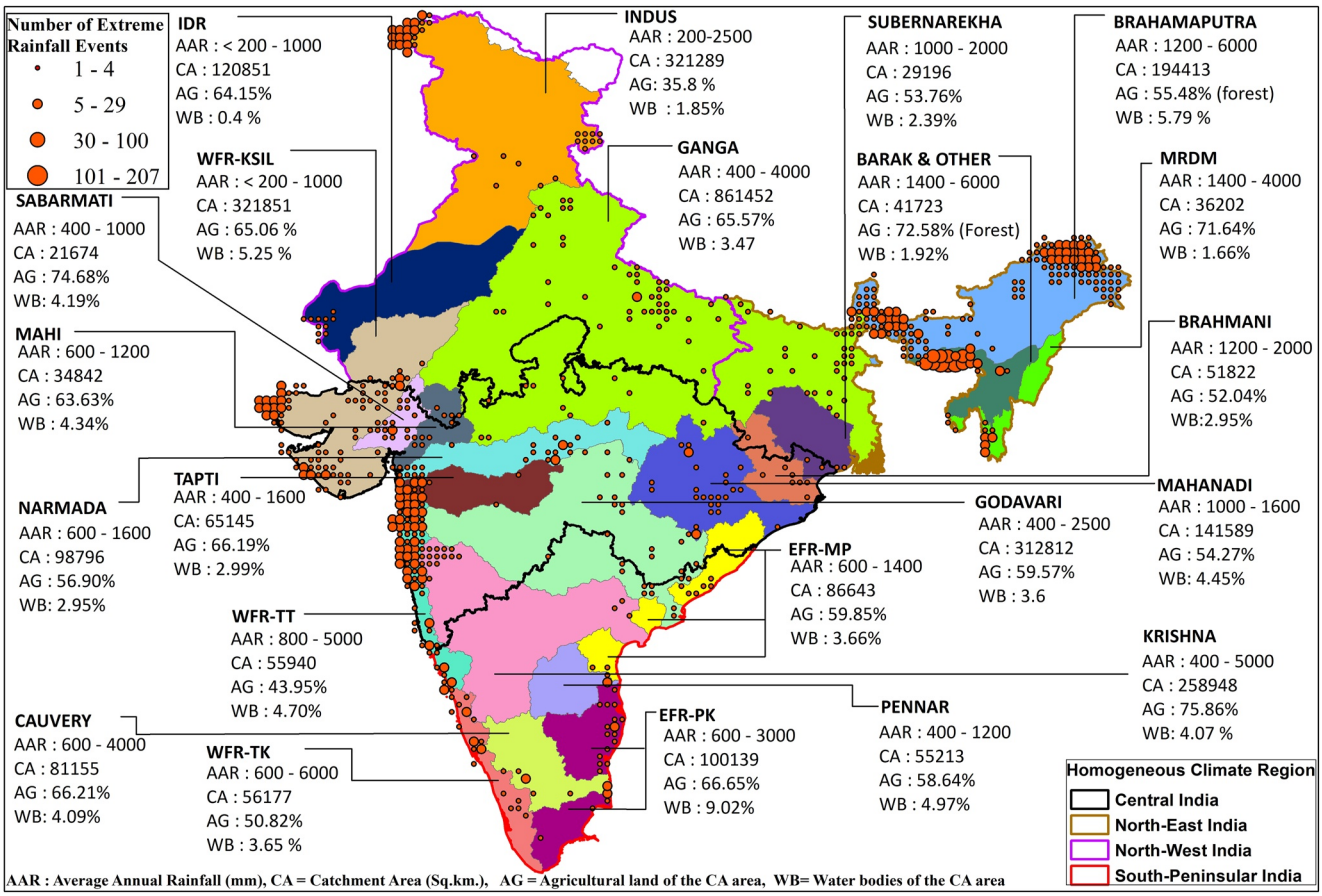

Figure 1. Overview of the Indian River Basins (IRBs). The red circle represents the hotspot as the number of extreme rainfall events at the 99.99th percentile (at the threshold value ≥300 mm day^{-1} rainfall) in 1901-2019.

2.2. Generalized Extreme Value (GEV) Distribution

The GEV distribution is used to estimate the return level of rainfall events at every grid point in the study. The GEV distribution is based on the block maxima theory and is used to compute the annual maxima of daily gridded rainfall to estimate the fitted GEV parameters; location (μ), scale (Ψ), and shape (ξ) parameters (Bhatia & Ganguly, 2019; Ghosh et al., 2012; Mannshardt-Shamseld in et al., 2012). Let's suppose R_m is the annual maximum of daily rainfall in the used rainfall series, then GEV distribution is defined as;

$$P_r\left(R_m \le R\right) = \exp\left[-\{1+\xi(R-\mu)/\Psi\}^{-1/\xi}\right] \quad (1)$$

Here, location and shape take a value between $(-\infty, +\infty)$, but the scale has to be greater than zero. To account for non-stationarity, the location and scale parameters are assumed to change with time. In this study, the location and logarithm of the scale parameter are modeled as polynomial functions of time. The three conditions for $\xi > 0$ is known as Frechet type, $\xi < 0$ is known as Weibull type, and $\xi = 0$ is known as the Gumbel distribution. The fitted GEV distribution is calculated using the maximum likelihood method by using the *fevd* function of the extRemes package in R at a 95% confidence interval. The outcomes from extremes value distribution with estimated parameters have been tested for statistical significance. The goodness of fit of the extreme value distributions has been performed using Kolmogorov-Smirnov at a 5% significance level. The applied GEV statistical methodology is detailed in Coles (2001), although the methodology related to climate application is deliberated in detail (Coles et al., 2003; Ghosh et al., 2012; Herold et al., 2017; Kao & Ganguly, 2011).

The n-year return value is defined by setting Equation 1 as [1-(1/n)], so the equation becomes:

$$1/n = \left[1+\xi\left(R_n-\mu\right)/\Psi\right]^{1/\xi} \quad (2)$$

Table 1
Definitions of Expert Team on Climate Change Detection and Indices Indices Used in this Study. (PR = Precipitation)

ETCCDI indices name	Indices	Unit	Definition
Annual total wet-day PR	PRCPTOT	mm	Sum of daily PR ≥ 1.0 mm
Contribution from moderate wet days	R75pTOT	%	Annual total rainfall when daily wet day amount >75th percentile (%); 90th percentile (%); 95th percentile (%); 99th percentile (%); (100*r99p/PRCPTOT)
Contribution from heavy wet days	R90pTOT		
Contribution from very heavy wet days	R95pTOT		
Contribution from extremely wet days	R99pTOT		
Max 5-day PR	Rx5day	mm	Annual max consecutive 5-day rainfall
Number of 5-day PR	R5day	days	Number of 5-days heavy PR
Number of heavy rain days	R10 mm	days	Annual number of days when PR ≥ 10 mm
Simple Daily Intensity Index	SDII	mm/d	Annual total PR divided by the number of wet days (when total PR ≥ 1.0 mm)

$$R_n = \begin{cases} \mu + \Psi n^{\xi} - \frac{1}{\xi}, & if \quad \xi \neq 0 \\ \mu + \Psi \ \log n \ , & if \quad \xi = 0 \end{cases} \tag{3}$$

Also, the n-year return value is a value that is supposed to occur once in n years under a stationary climate. The n-year return level is determined as an element of the location, shape, and scale parameters representing the annual maximum rainfall events at the (1/n) % probability of exceedance. Hence, for this research, we take the 10-, 30- and 100-year return levels are represented as the supposed intensity of 10%, 3.3%, and 1% probability of rainfall events. Furthermore, we would assume that at least one rainfall event occurs with 10%, 3.3%, and 1% probability in any given year. Return level calculation is done for every grid point of IMD rainfall datasets. It is also calculated on the extracted annual maxima rainfall within the basin shapefile of all 22 major river basins of IRBs.

2.3. Extreme Indices

To illustrate extreme rainfall, we used indices developed by the Expert Team on Climate Change and Detection Indices (ETCCDI; Zhang et al. [2011]), listed in Table 1. The ETCCDI climate indices are calculated using CDO to describe the extreme rainfall changes in the IRBs. The ETCCDI indices are used to estimate the spatial extent of rainfall extremes considering their significance toward frequency and intensity. The ETCCDI indices categorize the rainfall extremes from moderate to extreme events that occur multiple times per year and once per year, respectively (Herold et al., 2017). The ETCCDI indices are used to estimate the indices annually based on daily grid-based rainfall frequency. Some of the grid-cells within IRBs failed to process the GEV fit and ETCCDI indices, which is excluded from the study's calculation.

The Standardized Precipitation Index (SPI) is a probability (i.e., statistical) index representing abnormal wetness and dryness. The decadal changes in SPI at 12- months running window is used to compare the dry to wet condition across IRBs. According to (Trenberth et al., 2014), the SPI is based on only rainfall values, and the outcomes show the rainfall amount present in the area. To calculate and plot the SPI variation over the IRBs, we used NCAR Command Language (NCL) based on fitting a gamma distribution to monthly rainfall values using the function dim_spi_n (https://www.ncl.ucar.edu/Document/Functions/Built-in/dim_spi_n.shtml).

According to Rooy (1965), the Rainfall Anomaly Index (RAI) assign the rank of the rainfall values as per the equation given as

$$\text{RAI} = \pm SF \times \ [(p_i - \ \bar{p}) \div (\bar{m} - \bar{p})] \tag{4}$$

Where, p_i represents the monthly precipitation sum of the month i, $\bar{p}$ is the long-term average rainfall, $\bar{m}$ is the mean of the 10 highest or lowest values of precipitation (p), $\pm SF$ is the arbitrary threshold values of +3 and −3, respectively. These threshold values have been assigned to the mean of the 10 most extreme positive and negative anomalies (Table 2). The rainfall anomaly is the percentage departure of monthly rainfall from the long-term

Table 2
SPI and RAI Classification According to Their Original Definitions as Applied in this Study

S.No.	SPI (McKee et al., 1993)	Description	RAI (Van Rooy 1965)
1.	≥2.00	Extremely wet	≥3.00
2.	1.50 to 1.99	Very wet	2.00 to 2.99
3.	1.00 to 1.49	Moderately wet	1.00 to 1.99
4.	0.50 to 0.99	Slightly wet	0.50 to 0.99
5.	−0.49 to 0.49	Near normal	−0.49 to 0.49
6.	−0.99 to −0.50	Slightly dry	−0.99 to −0.50
7.	−1.49 to − 1.00	Moderately dry	−1.99 to −1.00
8.	−1.99 to −1.50	Very dry	−2.99 to −2.00
9.	≤−2.00	Extremely dry	≤−3.00

mean, which provides a dimensionless measure of the abnormal precipitation (Bhalme & Mooley, 1980; Hänsel et al., 2016). Table 2 shows the range value of SPI and RAI used in this study.

The study computes the grid-based percentage departure of realized rainfall from average rainfall. The percentage departure of rainfall for an individual year at every grid point was expressed as:

$$\%\ \text{Departure} = \left(\frac{\text{Annual rainfall for an individual year} - \text{Average of longterm annual rainfall}}{\text{Average of longterm annual rainfall}}\right) 100 \quad (5)$$

The percentage departure is classified as excess, normal deficient, or scanty as defined by IMD (Met Glossary). The probability distribution of the rainfall, percentage departure, and rainfall anomaly over the different IRBs is computed using Probability Density Function (PDF).

The intensity of the extreme rainfall events is computed based on the grid-wise rainfall distribution and categorized as per IMD criteria (http://www.imdpune.gov.in/Weather/Reports/glossary.pdf). According to that, the intensity of rainfall events between 64.5 and 124.4 mm day^{-1} is considered as heavy rainfall (HR), the rainfall events between 124.5 and 244.4 mm day^{-1} is considered as very heavy rainfall (VHR), and the rainfall events are greater than and equal to 244.5 mm day^{-1} is considered as extremely heavy rainfall (EHR).

2.4. Statistical Trend Test

Mann–Kendall (Kendall, 1948; Mann, 1945) trend test is a non-parametric rank-based trend test used to estimate any upward or downward trend present in a climate and hydrology time series data against randomness. It has been widely used for trend analysis in hydroclimatic studies and found to be a robust tool for trend detection in the distribution of hydro-climate variables and events (Ali et al., 2019; Hänsel et al., 2016; Papalexiou & Montanari, 2019). Hence, in the present study, authors have used it to determine the long-term trend present in the frequency of extreme rainfall events over India at a 5% significance level. Furthermore, the trend analysis performed at every grid point is carried out using the Mann–Kendall trend test method to consider linear trends. Sen's method is used to estimate the slope of the trend. The equations used in this research is:

$$S = (r_j - r_i)/(j - i), \quad \text{for}(1 <= i < j <= n) \quad (6)$$

where, S denotes the linear rate of change, that is, slope, r is the rainfall data, n time period of the data, and i, j are indices. Sen's slope is estimated from the slope's median as Sen(k) = Median(S). The median of these N number of pairs of time series elements estimates the nonparametric slope β as:

$$\beta = S\{(N+1)/2\}, \quad \text{for } N \text{ is odd}, \quad (7)$$

$$\beta = ½[S(N/2) + S\{(N+2)/2\}, \quad \text{if } N \text{ is even} \quad (8)$$

A 1–α confidence interval for Sen's slope can be calculated from the lower (L) and upper (U) limit of the slop, where

$$U = 1 + (N + C\alpha)/2, \quad \text{and} \quad L = (N - C\alpha)/2 \tag{9}$$

$$\text{Here,} \quad C\alpha = Z1 - \alpha/2\,\{\text{Var}(Sn)\}\,1/2 \tag{10}$$

And Z1- α/2 is the 100 (1-α/2) percentile of the standard normal distribution. A 100 (1-α) % confidence interval on the actual slope is lying as $L \leq \beta \geq U$.

3. Results and Discussion

3.1. Rainfall Distribution Over the IRBs

We first examined rainfall probability over different IRBs, followed by respective percentage departure and rainfall anomaly (Figure 2). According to the rainfall pattern, the study has classified four subclasses of the IRBs as NW-IRBs, NE-IRBs, CI-IRBs, and PI-IRBs (Figure 2).

3.1.1. North-West India River Basins (NW-IRBs) and North-East India River Basins (NE-IRBs)

The NW-IRBs are comprised of homogenous regions of the Indian river basins such as Inland drainage in Rajasthan (IDR), Indus, and the northwest part of the Ganga river basin. However, NE-IRBs included the Brahmaputra, Minor river draining to Myanmar (MRDM), Barak & other (BAO), and northeast part of Ganga river basins.

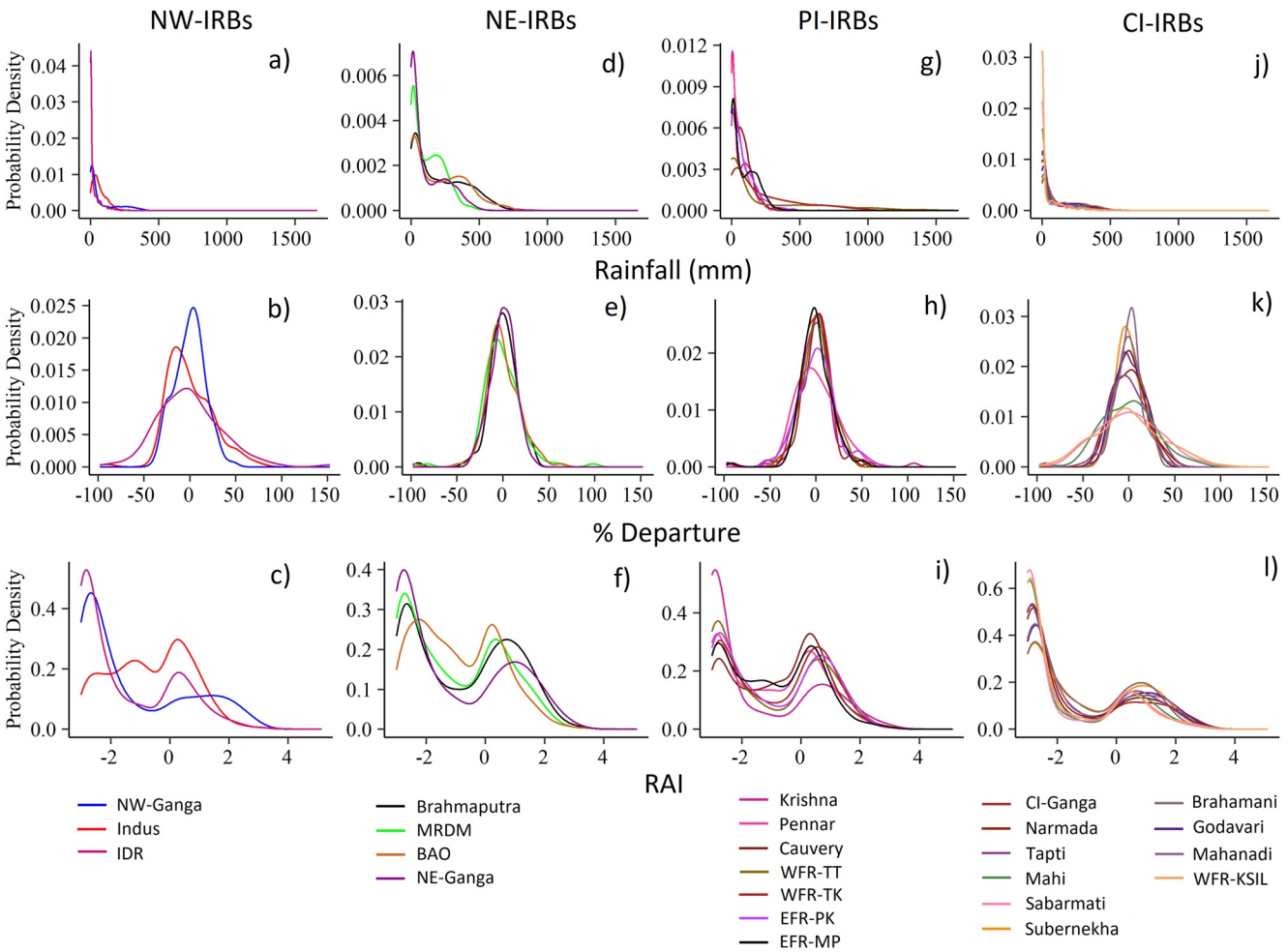

Figure 2. Probability distribution of monthly sum rainfall, percentage departure, and the rainfall anomaly over the North-West India river basins, North-East India river basins, Peninsular India river basin, and Central-Indian River Basins.

Figure 2a depicts that the probability of monthly sum rainfall of about 0–300 mm/months is highest in the Indus of NW-IRBs. However, Figure 2d shows a high probability of monthly sum rainfall 0–300 mm/months in MRDM and BAO about 300–500 mm/months over the NE-IRBs. Figure 2b shows the probability of deficiency in monthly rainfall departure (<−20%) is highest for Indus. However, the probability of average monthly rainfall departure (−19%–20%) has been observed NW-Ganga river basin (Figure 2b). The excess monthly rainfall departure (>20%) has been observed over the Brahmaputra and NE-Ganga river basins (Figure 2e). Figures 2c and 2f show the high probability (>0.2%) of rainfall anomaly ($0 \leq RAI \geq 1$) in the Indus of NW-IRBs and BAO of NE-IRBs, respectively. Moreover, NW-Ganga has a high probability of rainfall anomaly ($RAI \geq 2$; Figure 2c), while Brahmaputra of NE-IRBs has been observed the highest probability of rainfall anomaly ($0 \leq RAI \geq 2$; Figure 2f).

3.1.2. Central India River Basins (CI-IRBs) and Peninsular India River Basin (PI-IRBs)

The CI-IRBs are comprised of Narmada, Subernarekha, Brahamani, Mahanadi, Godavari, Tapti, Sabarmati, Mahi, WFR Kutch & Saurashtra, including Luni (WFR-KSIL), and central part of Ganga river basins. However, EFR Pennar and Kanyakumari (EFR-PK), WFR Tapti to Kanyakumari (WFR-TK), WFR Tapti to Tadri (WFR-TT), EFR Mahanadi and Pennar (EFR-MP), Pennar, Krishna, Cauvery river basins come under PI-IRBs.

The high probability of monthly sum rainfall (300–1000 mm) has been observed in WFR-TT and WFR-TK in PI-IRBs (Figure 2g). Meanwhile, in the monthly sum rainfall distribution between 0 and 300 mm, the Narmada river basin shows a high probability among all CI-IRBs.The Mahanadi river basins of CI-IRBs were estimated high probability of average percentage departure (0 to +10%; Figure 2k). The Mahanadi river basin of CI-IRBs shows a high probability of average rainfall percentage departure (−10% to +10%); however, WFR-KSIL observed a high probability of excess rainfall departure (≥+50%; Figure 2k). In Figure 2i, the high probability of rainfall anomaly ($0 \leq RAI \geq 1.5$) indicates normal to the slightly wet condition has been estimated Cauvery river basins of PI-IRBs. The extreme flood events in the Cauvery river basin crossed the danger level reported 127.83 m during the October months of monsoon season in years 2017-18 (CWC-2019). Also, out of all river basin of CI-IRBs, only the Ganga river basin show a low probability (≤0.2%) at the positive range of rainfall anomaly ($0 \geq RAI \leq 1.5$; Figure 2l).

3.2. Frequency Distribution

Next, we analyzed the long-term frequency changes in extreme rainfall events from 1901 to 2019, on daily rainfall events exceeding at 90th (P-90), 93rd (P-93), 95th (P-95), and 99th (P-99) percentile to understand the significance of changes shown in the supplementary figure (Figure S1 in Supporting Information S1). A significant increasing trend in the frequency of the extreme rainfall events was observed over Indus, the western part of the PI-IRBs, and NW-IRBs in events exceeding with 90th and 93rd percentile (Ali et al., 2019). About 45% of the IRBs show a significant increasing trend over the catchment area. Meanwhile, EFR-PK, Krishna, and Godawari river basins and the western part of the Ganga river basin estimated decline trend in rainfall extreme at 95% confidence interval (Figure S1d in Supporting Information S1). The frequency distribution trend of extreme rainfall was analyzed using the Mann-Kendall trend test with the 5% significance level.

3.2.1. Changes in the Frequency of Rainfall Events

This section presents the spatio-temporal changes in the frequency of extreme rainfall events at the grid-wise distribution of rainfall over the IRBs for long terms from 1901 to 2019 and 40-year time interval frame from 1901 to 1940, 1941 to 1980, and 1981to 2019. Figure S2 in Supporting Information S1 shows the spatial distribution of VHR and EHR events over the IRBs at 40 years's time intervals. Figure S2 in Supporting Information S1 a shows large variability in the total rainfall maxima of EHR events across the IRBs: the largest over the Ganga and the smallest over the Cauvery and Pennar river basins have been observed during 1981-2019. The spatial sum of the number of extreme rainfall in all 22 major IRBs is listed in Table 3. The Ganga, Brahmaputra, and BAO river basins recorded the maximum number (>1000) of EHR events (Table 3). Figures 3a–3c show that the largest number of HR to EHR events are concentrated over the west-flowing river basins of the PI-IRBs, including WFR-TT, WFR-TK, and EFR-PK, and these events are mainly located along hilly regions of the PI-IRBs (Deshpande et al., 2016). However, both EHR and VHR events were observed in the NW-IRBs river basins, while HR events were deficient. The CI-IRBs experienced more HR events instead of EHR events, while IDR, Krishna, and Cauvery showed none of the EHR events (Figure 3).

Table 3
Extreme Rainfalls Distribution Over the 22 Major IRBs of India

S. No.	Indian river basins (IRBs)	119 years spatial sum of number of rainfall extreme events			Return level (mm)		
		Heavy rainfall (64.5-124.4)	Very heavy rainfall (124.5-244.4)	Extreme rainfall (≥244.5)	10-year	30-year	100-year
1	Indus	42,420	5046	328	1023	1229	1454
2	Ganges	221,556	31,485	1351	1217	1361	1519
3	Brahmaputra	138,495	20,056	1182	3006	3389	3809
4	Brahmani	17,756	2822	149	1755	1978	2223
5	Cauvery	11,733	1315	100	1113	1276	1456
6	Godavari	77,695	11,590	547	1349	1537	1742
7	Mahandi	48,659	8092	404	1645	1868	2111
8	Mahi	10,898	2459	148	1177	1444	1736
9	Narmada	30,896	5583	314	1389	1618	1870
10	Pennar	6573	884	45	905	1072	1256
11	Sabarmati	7409	1588	181	1077	1349	1647
12	Tapti	15,911	2861	208	1124	1320	1535
13	Krishna	33,362	3988	219	1149	1438	1756
14	Subernarekha	19,839	2918	159	1674	1894	2134
15	Inland drainage in Rajasthan (IDR)	5701	705	44	429	544	669
16	WFR Kutch & Saurashtra Including Luni (WFR-KSIL)	28,723	6747	670	722	917	1131
17	WFR Tapti to Tadri (WFR-TT)	69,065	17,153	1001	3368	3856	4391
18	WFR Tapti to Kanyakumari (WFR-TK)	52,129	7995	325	3346	3812	4322
19	EFR between Pennar and Kanyakumari (EFR-PK)	21,320	3467	223	2525	3036	3596
20	EFR Mahanadi and Pennar (EFR-MP)	16,594	2852	166	1302	1487	1690
21	Minor River draining to Myanmar (MRDM)	7643	884	71	1966	2333	2735
22	Barak & Other (BAO)	31,766	7185	1824	3146	3655	4213

Figure S3a-c in Supporting Information S1 shows high spatial variations in the frequency of rainy days (rainfall ≥2.5 mm) at the threshold percentile level at 99.50, 99.97, and 99.99. The west-flowing river basins of PI-IRBs and NE-IRBs were evaluated with the highest number of rainy days at the threshold frequency as 99.50 percentile. Figure 3g-f shows the 5-day accumulated rainfall, which is the highest sum of consecutive 5-day rainfall at the 95th, 99th· and 99.50th percentile over the IRBs. The highest count of 5-day rainfall sum at the 95th and 99th percentile threshold over the NE-IRBs and west-flowing river of PI-IRBs, causing a flash flood situation over the basins (Dash et al., 2009). The WFR-KSIL, WFR-TT, WFR-TK, and CI-IRBs, including Narmada, Mahanadi, the eastern part of the Godavari, have been observed to have the highest count of VHR, having a threshold of 99th percentile at 5-day rainfall. These findings are consistent with that of Goswami et al. (2006) (Figure 3h). However, the EHR at the 99.50 percentile of the 5-day accumulated rainfall shows a scattered pattern all over the IRBs. Moreover, the highest number was recorded in BAO and WFR-TT (Figure 3f).

At the 40-year time interval, the intensity of heavy, very heavy, and extreme rainfall distribution for 1901-1940, 1941-1980, and 1981-2019 (Figure 4). During the recent period 1981-2019, EHR events have risen spatially in widespread new grids over the WFR-TT and lower Narmada basin. The highest number of heavy rainfall events were observed over the Mahanadi river basin and the lower part of the Ganga river basin. Figure 5 shows the decadal variation of HR to EHR between 1981 and 2019. The CI-IRBs part containing WFR-TT, Narmada, and the Godavari river basins shows a rise in the intensity of HR events during 1981-2019. The significant rise in the intensity of HR events over the CI-IRBs included Godavari and Narmada–Tapi river basins (Deshpande et al., 2016; Goswami et al., 2006). In the 80 and 90s decades of the twentieth century, additional grids showed an increase in extreme rainfalls all over the IRBs. In contrast, in the recent decades of the twenty first century, the maximum number of extreme

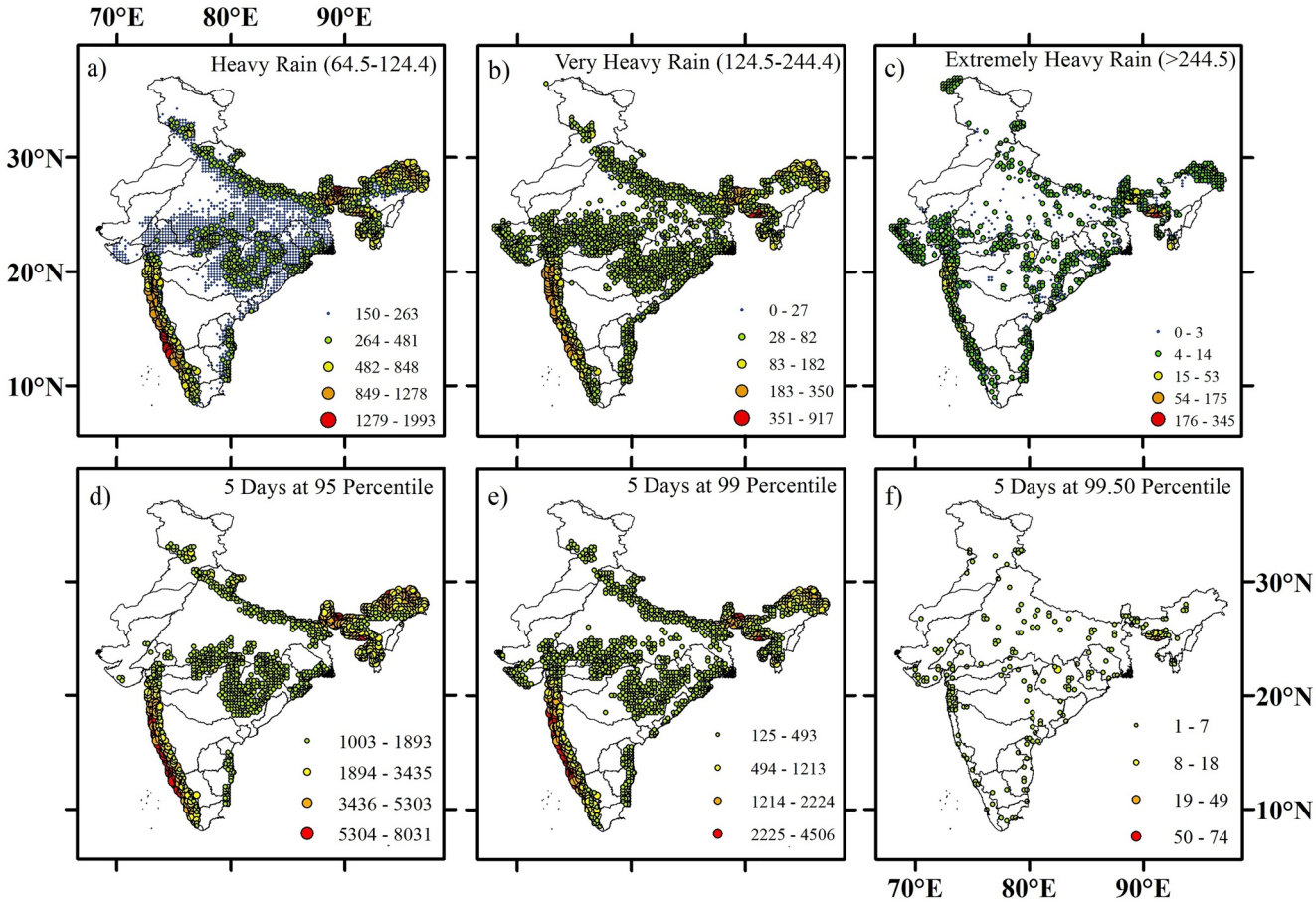

Figure 3. Long-term (1901-2019) observed number of extreme rainfall according to Indian Meteorological Department criteria for the intensity of rainfall, (a) heavy rainfall (HR), (b) very heavy rainfall (VHR), and (c) extremely heavy rainfall (EHR). Figure (d)–(f) represents accumulated 5 days at 95, 99, and 99.50 percentile having threshold greater than and equal 124, 233, and 292 mm/5 days rainfall, respectively.

rainfall events were observed over the WFR-TT and BAO and the lower part of the Mahanadi and Godavari basins. However, WFR-KSIL experienced the maximum number of EHR events over the basin last 9-year (2011-2019).

3.3. ETCCDI Indices Estimation

To analyze these extremes further, we use ETCCDI indices over the IRBs, which are important in identifying the low and high-risk river basin area in terms of frequency and intensity of extreme rainfall. The changes in the intensity and frequency of rainfall over the IRBs at threshold percentile 75th, 90th, 95th, and 99th are listed in Table 1. Moreover, moderate to extremely wet days were calculated using ETCCDI indices R75pTOT, R90pTOT, R95pTOT, and R99pTOT (Figures 6a–6d). In Figure 6a, the IDR, Indus, northern region of the WFR-KSIL, and northwest part of the Ganga river basins show the changes between 59% and 99% rainfall at the R75p (rainfall at 75th percentile) while EFR-PK and some of the eastern regions of the Cauvery basin were showed 46%–73% rainfall at the moderate wet days. Moreover, 75%–80% of wets days above the 90th percentile were estimated over the Ganga river basin, the western part of the IDR, and the lower part of the Indus basin (Figure 6b). Figure 6d shows the spatial distribution of extremely wet (R99pTOT) days for the rainfall percentage above the 99th percentile as estimated over the IDR, WFR-KSIL, and MRDM river basins. Figures 6e–6h show the spatial pattern of the number of days having threshold 10 mm (R10 mm), 20 mm (R20 mm), 25 mm (R25 mm), and 35 mm (R35 mm) rainfall per day. The highest number of the count of daily rainfall amount at a threshold of 10–20 mm per day has been observed over the NE-IRBs, including the Brahmaputra and BAO as well as the west-flowing river basins of the homogeneous region of peninsular India (Figures 6e and 6f). These rainfall patterns supported

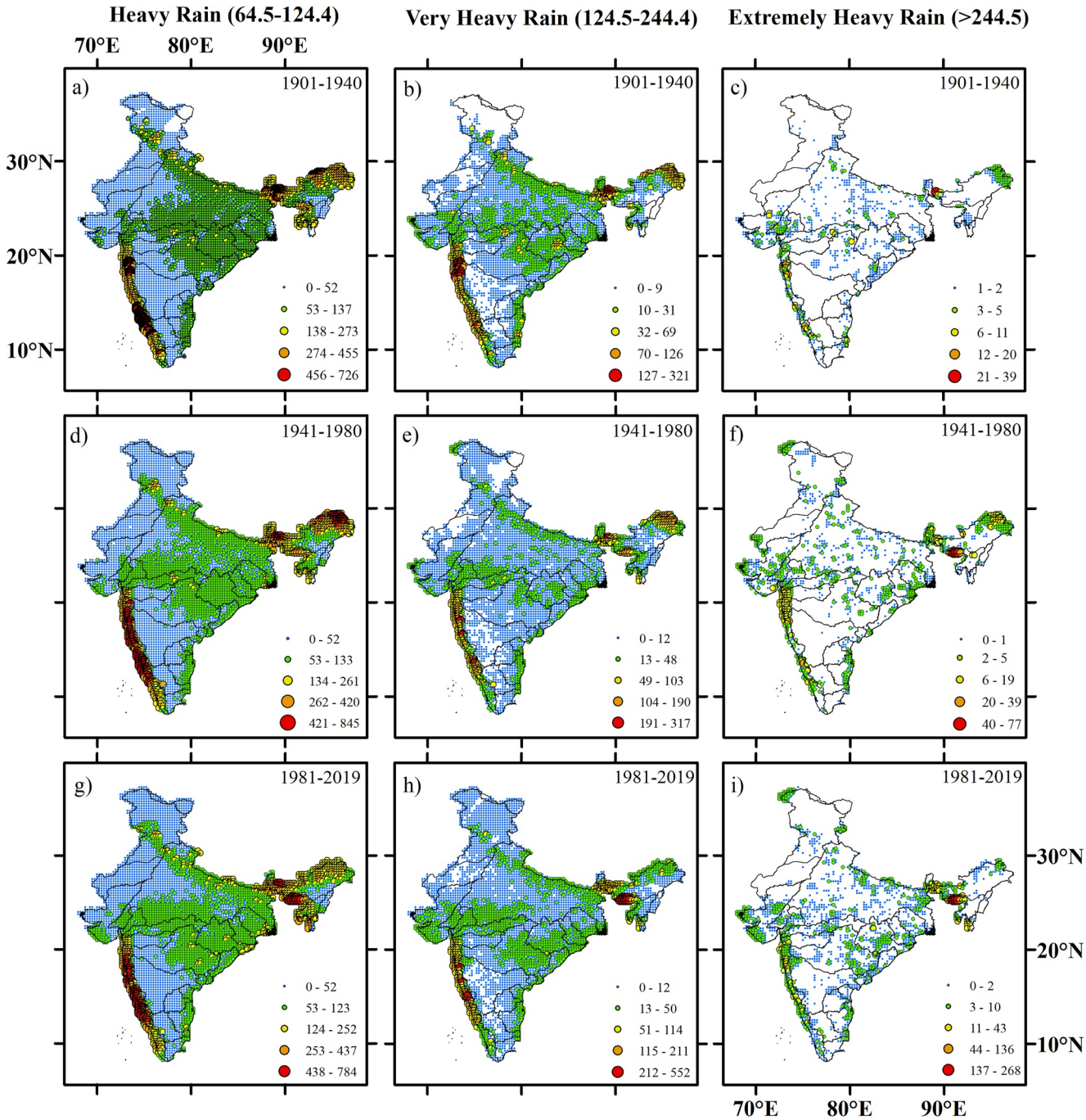

Figure 4. The number of extreme rainfall events for the heavy rainfall (HR), very heavy rainfall (VHR), and extremely heavy rainfall (EHR) to the time period 1901-1940 (a–c), 1941-1980 (d–f), 1981-2019 (g–i).

with the previous research resulted in the increasing HR events across the northeast and western parts of India, which may associate with north-ward and west-ward moving monsoonal depressions (Goswami et al., 2006; Roy & Balling, 2004).

East flowing river basins, including the lower part of the Godavari, Mahanadi, Brahmani, and Subernarekha, showed the maximum daily rainfall amounts at the threshold of 10 mm per day (Figure 6e). The previous study has concluded that the rainfall extremes are more dominant in northern and southern parts of India (Joshi & Rajeevan, 2006; Suman & Maity, 2020). The moderate to VHR percentile distribution over the 40-year running

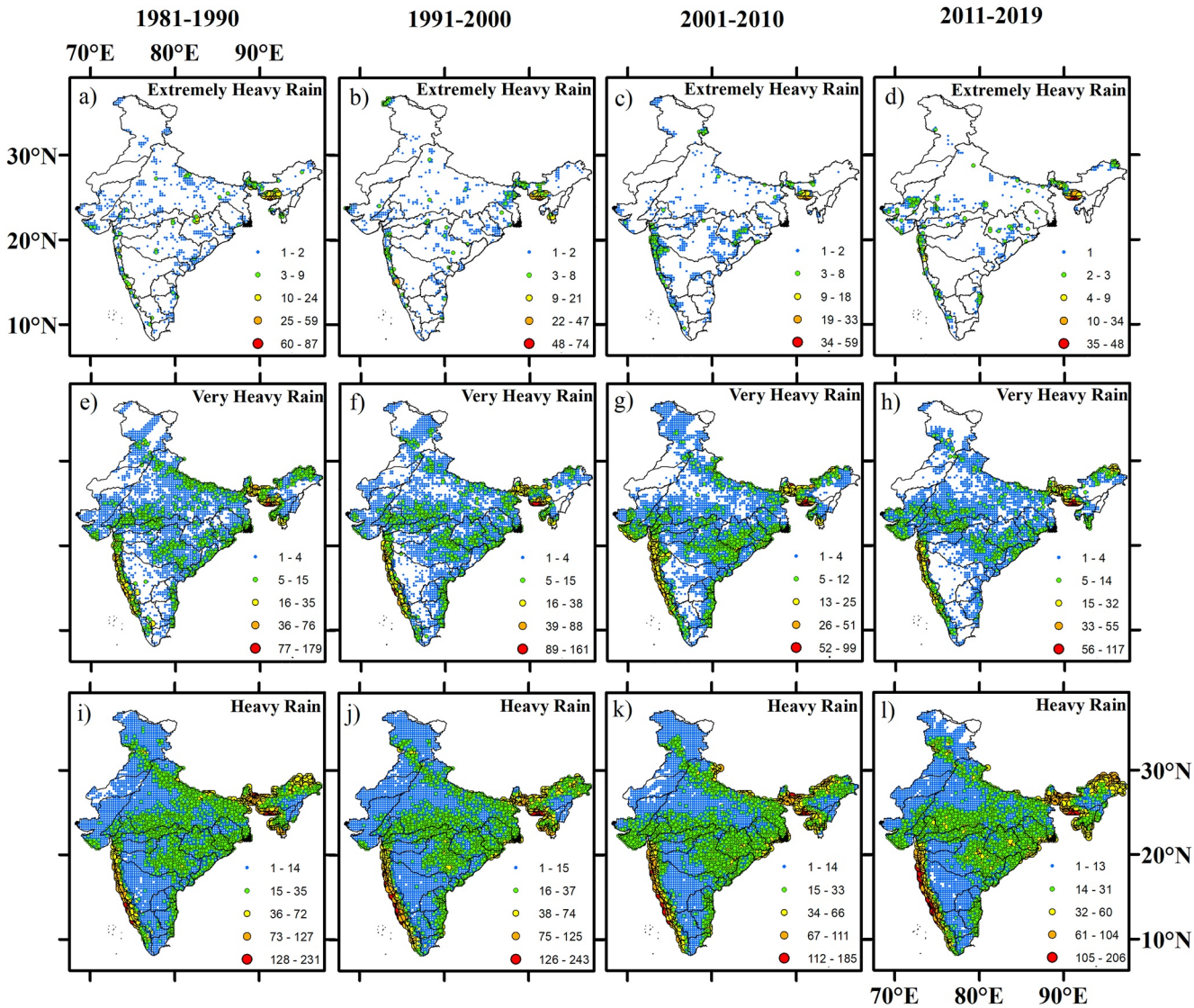

Figure 5. Decadal variation of the number of extreme rainfall events, (a–d) extreme heavy rainfall (>244.5 mm), (e–f) very heavy rainfall (124.5–244.4 mm), and (i–l) heavy rainfall (64.5–124.4 mm) for the decadal time period 1981-1990, 1991-2000, 2001-2010, and 2011-2019. Note Only 9 years of data analysis were done in the time period 2011-2019.

calculation was shown in Figure 7. The spatial variability of the 5-day maximum rainfall and the number of the 5-day rainfall over the IRBs has been shown in Figure 8a-f. The 5-day heavy rainfall events are caused by depression and cyclones created over the Bay of Bengal, usually 3–5 days's time period, and transport moisture toward the northwest (Roxy et al., 2017; Roy & Balling, 2004) of the IRBs. However, the variation of the number of rainfalls at 10 mm per day decreasing rate is estimated over the 40-year running time span (Figure 8g-i).

3.4. Return Periods and Spatial Variation of Rainfall Extremes Over IRBs

Next, we estimated the spatial distribution of the total annual maxima of the rainfall during 1901-2019 on every grid point. The return level was calculated based on observed annual rainfall for 10-year, 30-year, and 100-year return periods. The spatial distribution annual maxima rainfall extremes were estimated as the rainfall per day at the 10- years, 30-year, and 100-year return levels (Figure 9). India's central and peninsular homogeneous river basins show significant variation in rainfall extremes depending on the annual maxima at 10-, 30-and 100-year return levels based on EVT (Figure 9). In Figure 9b-c, the Indus, western lower part of the WFR-KSIL, Tapti, Godawari, and west-flowing river basins of peninsular India, the meanwhile north east belt of Ganga and

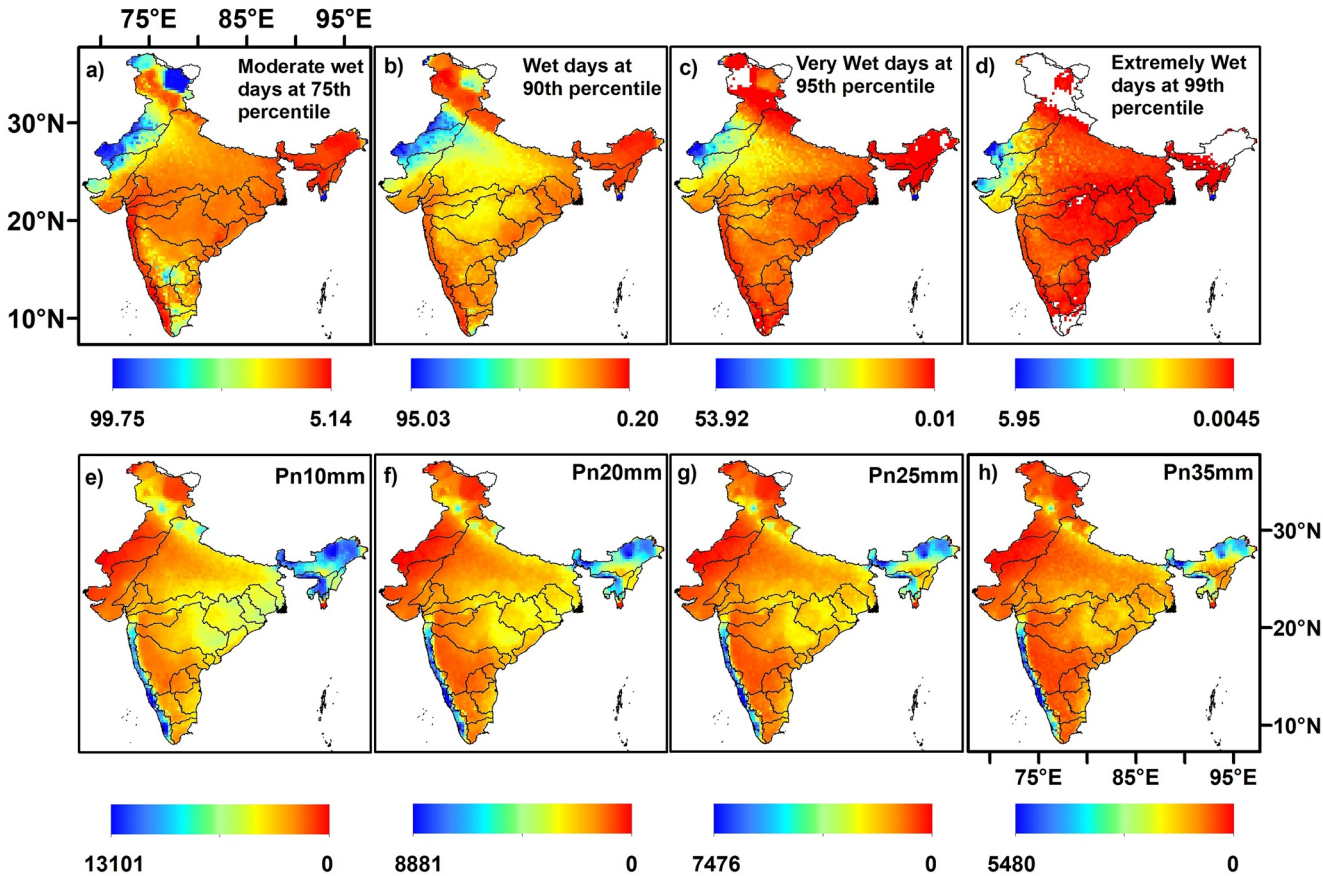

Figure 6. Spatial variation of rainfall using Expert Team on Climate Change Detection and Indices (ETCCDI) indices measure annual accumulated rainfall for events above (a) 75th (b), 90th (c), 95th, and (d) 99th percentiles as moderate to extremely wet days, respectively. The figure displays the annual count of days with a daily rainfall amount threshold is 10 mm (e), 20 mm (f), 25 mm (g), 35 mm (h). The ETCCDI indices have not processed the white part of the figure.

NW-IRBs show the expected 3.3% and 1% probability of extreme rainfall events in 30- and 100-year return level and is consistent with (Ghosh et al., 2012). Moreover, the separately basin-wise return level distribution has been calculated over all 22 major IRBs based on the total monthly rainfall values over the IRBs at 10-year, 30-year, and 100-year return periods (Figure S4 in Supporting Information S1). The trend as a covariate in the location and/or scale parameters if statistically significant trends are found. Figure S5 in Supporting Information S1 shows the grid-based trends at different return levels.

3.5. Shifting Pattern in Rainfall Over IRBs

Analysis of the long-term (1901-2019) and decadal trends of the rainfall at every grid cell in the IRBs at three time intervals 1901-40, 1941-80, and 1981-2019, for annual, monsoon, and non-monsoon months rainfall is being discussed in this section. The JJAS (June-July-August-September) has been selected as the monsoon months, while remaining months other than JJAS were selected as the non-monsoon months in this study. A significant increase and a spatio-temporal shift in the trend of occurrence of rainfall (94 ± 10 mm decade^{-1}) has been observed toward WFR-KSIL and WFR-TT at 95% confidence interval at the end of twentieth and beginning of the 21st century (1981-2019), as compared to early twentieth century (1901-1940). However, the upper part of the Ganga, Indus, Brahmaputra, and BAO show a significant increasing trend of 142 ± 9 mm decade^{-1} for 1981-2019 (Figure 10c). The monsoon rainfall (JJAS) variability is attributed to the inherent nonlinearity of the atmospheric dynamics that make it nonperiodic over the decades (Narayanan et al., 2016). The decadal trend of the annual and monsoon months rainfall shows a significant increasing trend over the northern part of the Brahmaputra and WFR-KSIL and WFR-TT during the time period 1901-2019. Analyzing the decadal shifting trend of the observed

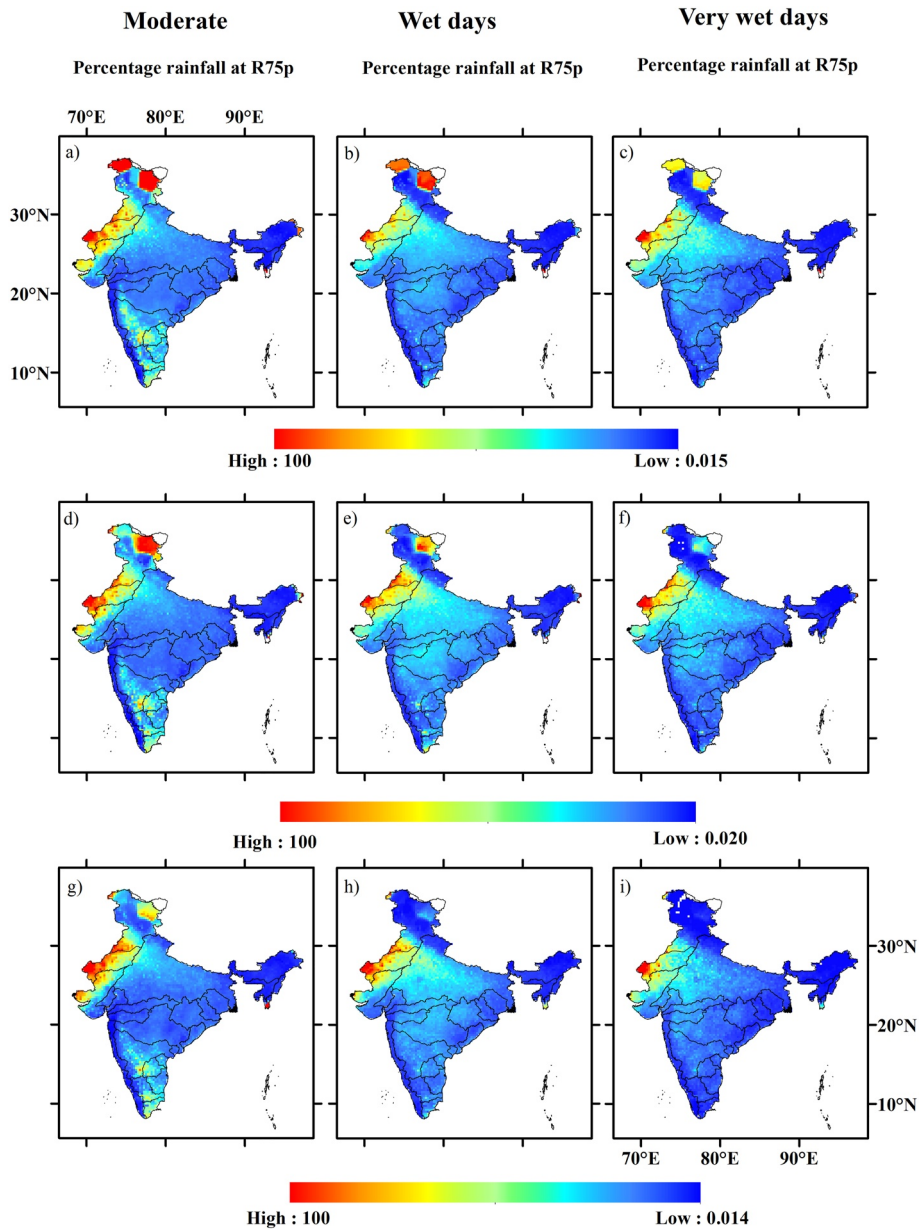

Figure 7. Spatial changes in the percentage rainfall estimated by using Expert Team on Climate Change Detection and Indices indices at 75th, 90th, and 95th percentile for moderate to very wet days over the Indian river basin at the 40 years's time interval from 1901 to 1940 (a–c), 1941-1980 (d–f), and 1981-2019 (g–h).

meteorological parameters like rainfall helps to understand the variable weather and hydro-climate extremes (droughts, floods, etc.) over the different IRBs and their long-term socioeconomic effects (Caporali et al., 2021).

As done by Rajeevan et al. (2008) and Roxy et al. (2017), we have directed the long term trend analysis for the occurrence of extreme rainfall considering a daily rainfall frequency of ≥150 mm day^{-1}, where HR and VHR are characterized as rainfall equal and greater than 64.5 mm day^{-1}and 124.5 mm day^{-1}, respectively (Figure S6 in Supporting Information S1). Figure S6a in Supporting Information S1 shows an increasing trend of rainfall all over the IRBs. However, WFR-KSIL, the western part of the Indus, the central part of the Krishna and Narmada, and the lower parts of the Ganges indicated a significant increasing trend in HR events at a 95% confidence interval. The rainfall extremes over the CI-IRBs and the Monsoon Trough (MT) region of India are associated with the active monsoon growing from moist convective processes and the south-westerly monsoon circulation

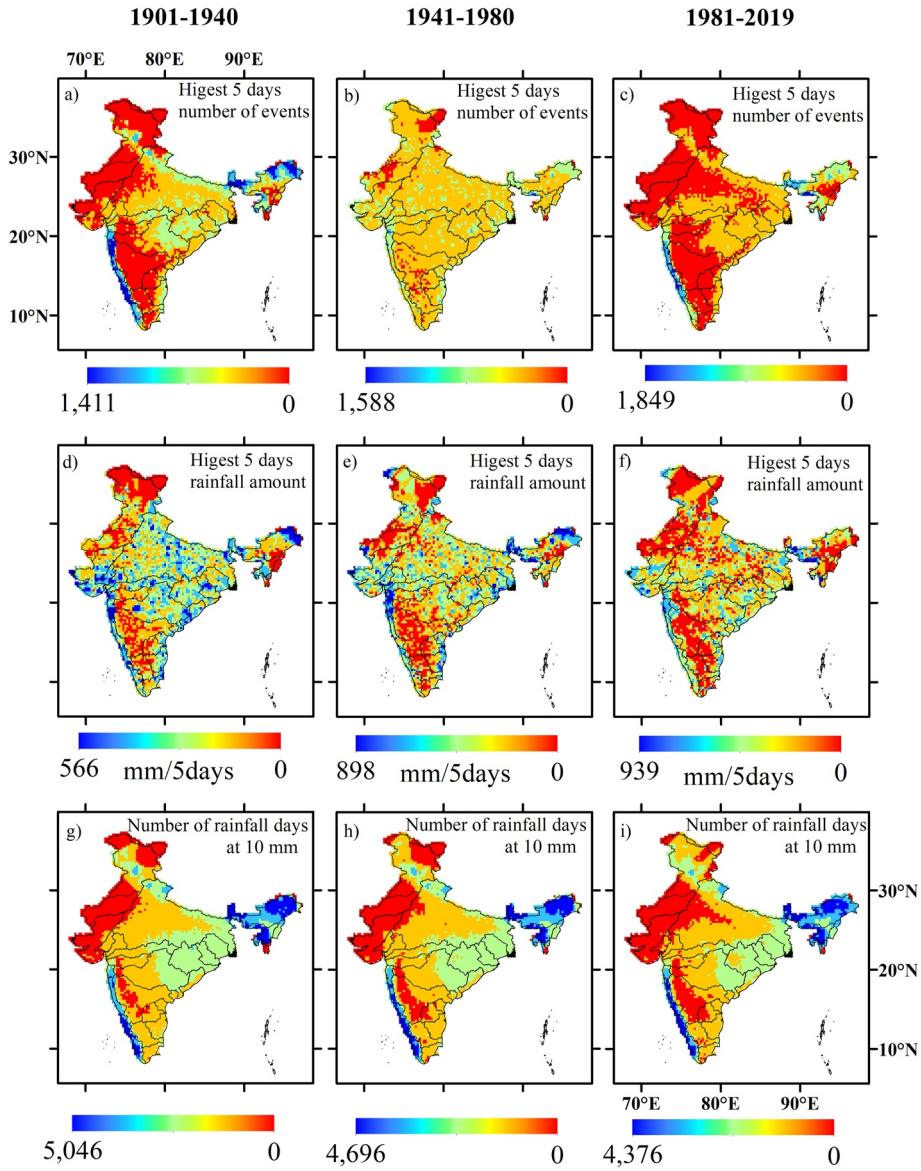

Figure 8. Spatial variability in the highest number of 5 days rainfall (a–c), maximum 5-day rainfall (d–f), and the number of rainfall days at 10 mm (g–i), estimated by using Expert Team on Climate Change Detection and Indices indices over the Indian river basins.

(Choudhury & Krishnan, 2011; Rajeevan et al., 2006). The Mahanadi & Narmada of the CI-IRBs, and BAO & MRDM of the NE-IRBs, showed an increasing trend of HR to VHR events (Figure S6a-b in Supporting Information S1). The estimated trend from 1901 to 2019 in the daily rainfall ≥150 mm day^{-1} shows an increasing trend over the WFR-TT and WFR-TK of the PI-IRBs, along with Mahi, Narmada, and Mahanadi of the CI-IRBs (Roxy et al., 2017). However, the increasing trend of EHR events in the downward western part of the Brahmaputra and BAO was observed in NE-IRBs (Figure S6c in Supporting Information S1).

Next, we examined the grid-based monthly rainfall trend, and the estimated values have been interpolated with the corresponding grid cells shown in Figure 11. The MK test has been applied to annual, monsoon, and non-monsoon months for the 40-year running time span. The monsoon rainfall shows the shifting trend of about 2 ± 1.08 mm JJAS^{-1} toward the NW-IRBs, including WFR-KSIL, Sabarmati, Mahi, and lower part of the Narmada basin, meanwhile about 3.08 mm JJAS^{-1} significant increasing trend in some part of the Indus river basin and upper part of WFR-TT of IRBs (Figures 11h). The annual (90 ± 6 mm year^{-1}) and monsoon rainfall show a positive

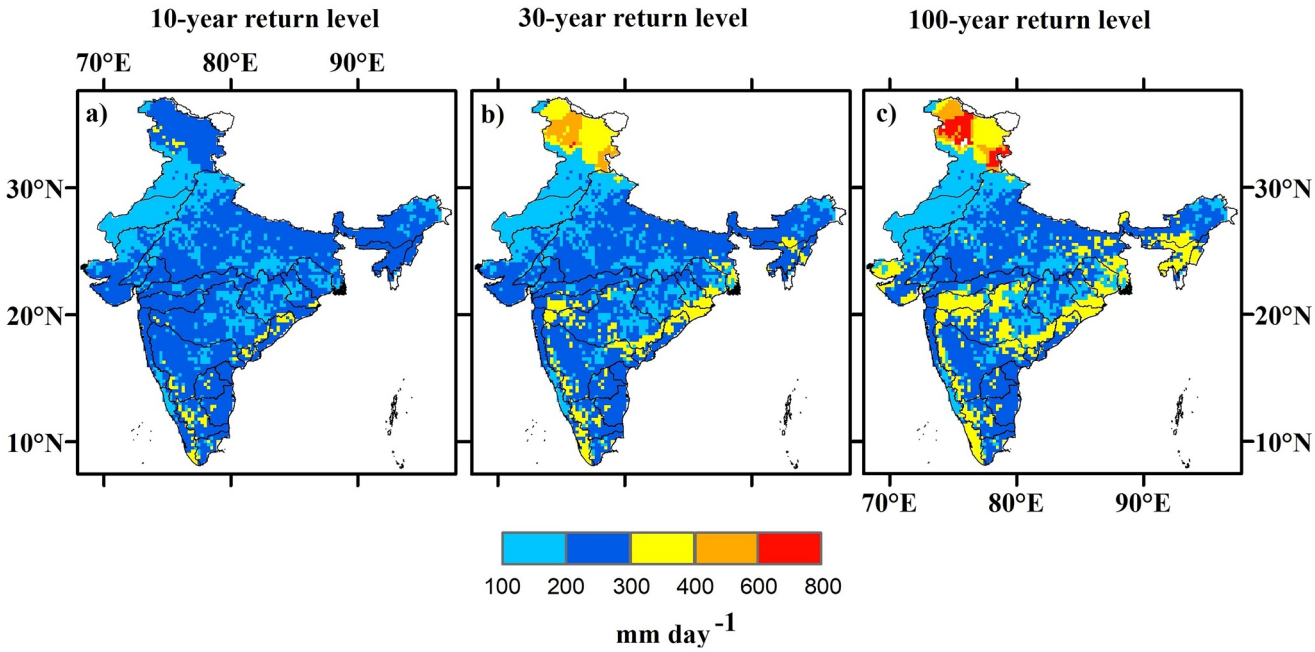

Figure 9. Spatial grid-based estimation of return level of rainfall extremes over the Indian river basins (IRB) at10-year (a), 30-year (b), and 100-year (c) return levels, using 1901–2019 data. The 10, 30, and 100-year return levels are interpreted as the expected intensity of 10%, 3.3%, and 1% probability storms, respectively. The white color over the North-West-IRBs, Minor river draining to Myanmar, and Indus river basin represents the unprocessed data sets.

shifting pattern in rainfall trends over the west-flowing rivers, including WFR-KSIL, WFR-TT, the lower part of the Narmada, and Mahi during 1981-2019. The research was done by Suman and Maity (2020) resulted that the changes in moisture flux will increase in eastward winds over South India and the Bay of Bengal, which is directly associated with the strengthening of the positive phase of Indian Ocean Dipole (IOD; Cai et al. [2014]). The change in moisture flux enhanced the potential of warm air in carrying the water, the convergence of moisture, etc., are identified as the contributing factors in the changes in extreme rainfall events (Donat et al., 2016; Suman & Maity, 2020; Trenberth et al., 2014). Shifting in rainfall increased the extreme rainfall events in the last two decades and resulted in damage to life and property on the west coast, including Mumbai. Meanwhile, no significant changes were detected in non-monsoon rainfall.

We further estimated the decadal changes in average intensity of dry and wet conditions at 12- months running time window (Figure 12). During the 1901-1940 era, the Cauvery and EFR-PK river basins of the PI-IRBs show slightly to a very wet state ($0.5 \leq SPI \leq 2$), and Brahmani shows the extremely wet state ($SPI \geq 2.5$) during the decades 1901-1910 and 1931-1940. Meanwhile, high drought intensities ($-3 \leq SPI \geq -0.5$) were observed over the Godawari and Krishna river basins. The WFR-KSIL and IDR river basins showed a moderate to extremely dry state ($-2 \leq SPI \geq -0.5$) in the decades 1911-1920. During the period 1941-1980, the decades 1941-1950 and 1971-1980 showed the moderate wet to a very wet condition in the Indus and central part of the Ganga river basin having SPI between $1 \leq SPI \geq 2$, whereas very to extreme wet condition ($1 \leq SPI \geq 2$) over the WFR-KSIL during decades 1961-1970. However, during 1981-2019, drastic changes in SPI ($0 \leq SPI \geq 3$) were observed, indicating a shift in extreme rainfall events toward the central-western part of the IRBs. The output of the research conducted by Chase et al. (2003) indicated global climate shift and the deterioration of monsoon circulation globally as the prominent factor behind rainfall shift since the 1970s. The significance of this shift has a direct consequence on the climate indices and the frequency of the cyclone over the Bay of Bengal and Arabian Sea (Narayanan et al., 2016; Singh et al., 2001).

During the period 1901-1940 and 1941-1980, the IDR, WFR-KSIL, WFR-TT, Mahi, Narmada, and lower southwest part of the Ganga river basin show the moderate dry to slightly wet condition while during the time frame 1981-2019, these basins show moderate wet to extremely wet condition. And the research done by Ratna et al. (2021) confirmed that in the last two decades and the last 38 years, India experienced the strongest IOD, which was conducive to extreme rainfall. The two decades 2001-10 and 2011-19were amongst the wettest decades compared to 1901-2000. Moreover, this indicated a shifting pattern (4%–50.87% change) in wet conditions over

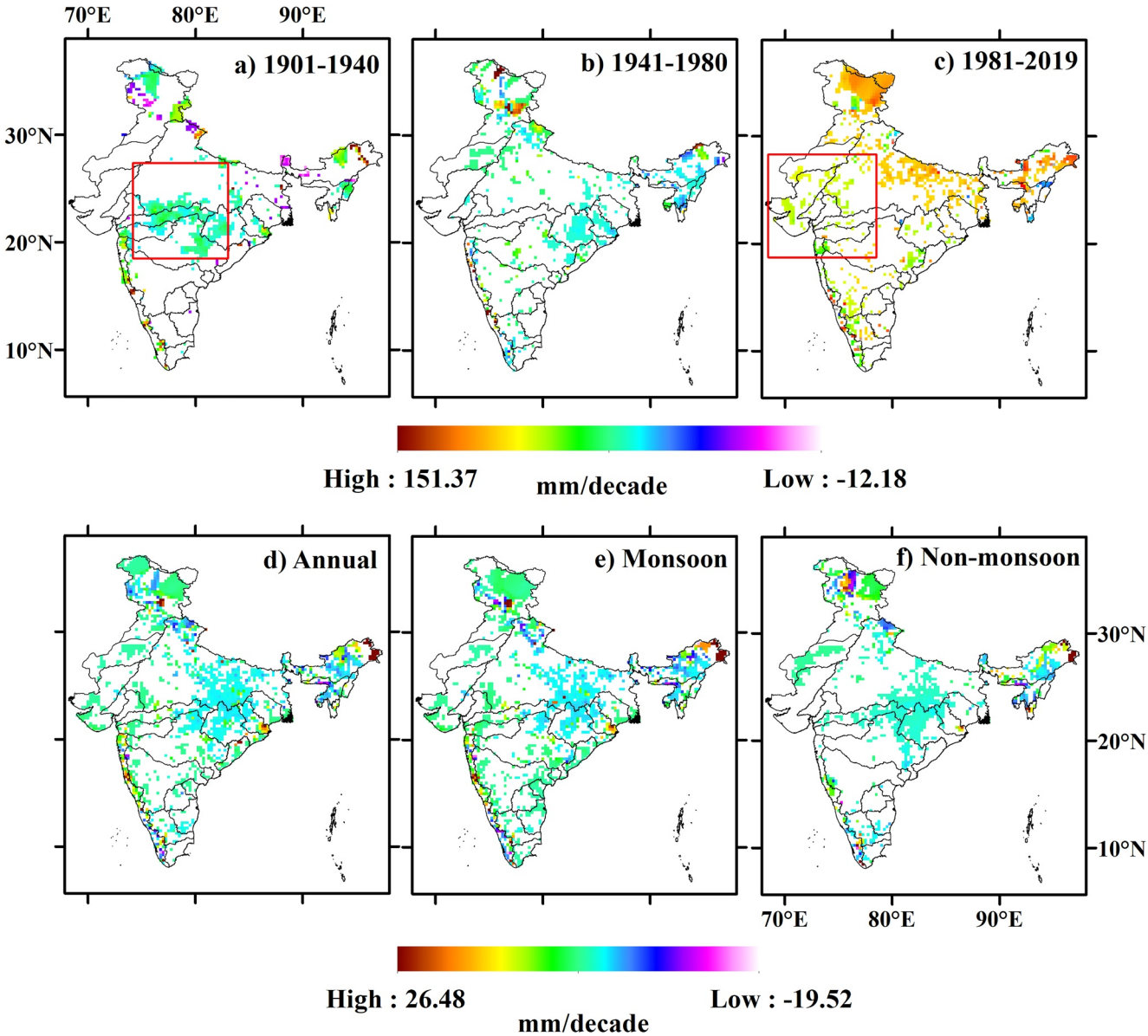

Figure 10. The decadal trend of spatial rainfall distribution at 40 years's time interval (a–c) in the red box shows the positive trend of rainfall over the Indian River Basins (IRBs). Decadal trend of rainfall for (d) Annual, (e) Monsoon, and (f) Non-monsoon at long-term monthly rainfall over the IRB. Figures (a–f) show only those values significant at 95% confidence level are shown.

the western river basins of IRBs (Figure 12). This shifting of the wet situation confirmed similar results of the recent study by Roxy et al. (2017), which reported an increase in extreme precipitation events over central India over the past half-century (1950-2015).

4. Conclusion

As discussed above, we found a spatial heterogeneity of the extreme rainfall events over the IRBs. The spatial heterogeneity reveals an increasing rate of rainfall extremes in IRBs, which may have resulted from local influences, such as topography, non-uniform population growth, and urbanization. The IRBs experienced successive good rainfall in the earlier 21st century compared to the mid-twentieth century, which amounts to about an 8% increase in mean rainfall anomaly above normal. The Ganga, west-flowing river basins of the homogeneous region of Peninsular India, and Northeast homogeneous river basins experienced the highest rate of spatial variability of extreme rainfall events in the last 39-year compared to the earlier and mid-twentieth century. The

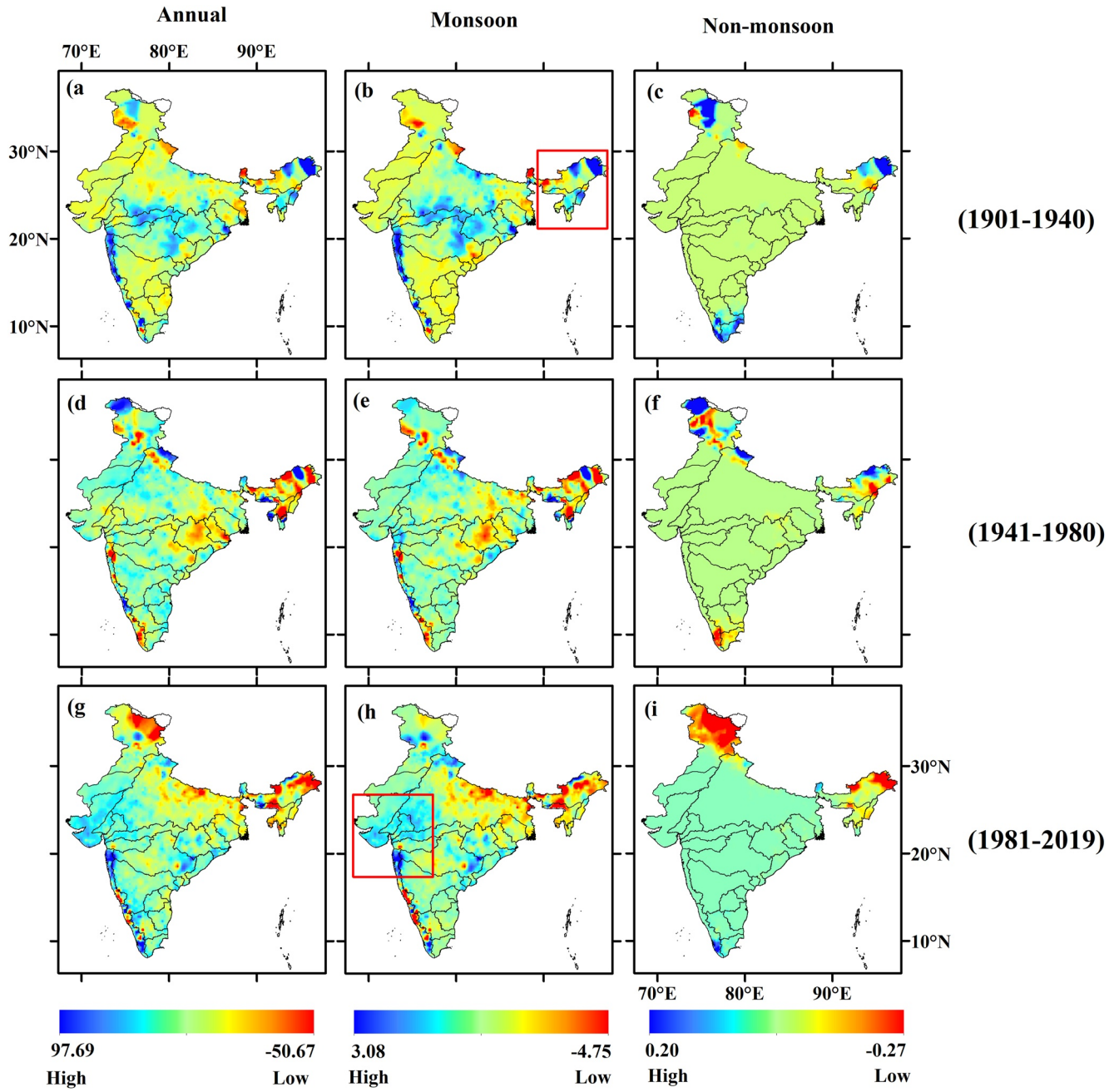

Figure 11. Shifting trend of the rainfall at the beginning of twentieth century (a–c) 1901-1940, (d–f) mid-twentieth century, and (g–i) last twentieth century and beginning of the 21st-century at 40-year time interval based on the observed rainfall period (1901–2019), the rectangular red box represents the shifting trend of the rainfall.

frequency of 5-day rainfall extremes events has decreased in the last 39-year as compared to the mid and earlier twentieth century, but an increased intensity in observed maximum 5-day rainfall values was observed in the last two decades of the twenty first century, which has intensified the flood hazards situation along the western ghats and western river basin of the IRBs. The 1% probability of the extreme event increased in the northern, western river basin system as well as the upper part of the Indus and Ganga river basin at the 100-year return period.

Meanwhile, rainfall extremes at the daily frequency over the homogenous region of the northeast and peninsular India at a 30- and 100-year return level was found. This study concluded that the western and central IRBs experienced increasing VHR to EHR events in the last 39 years. The study determined an increase in the extreme events

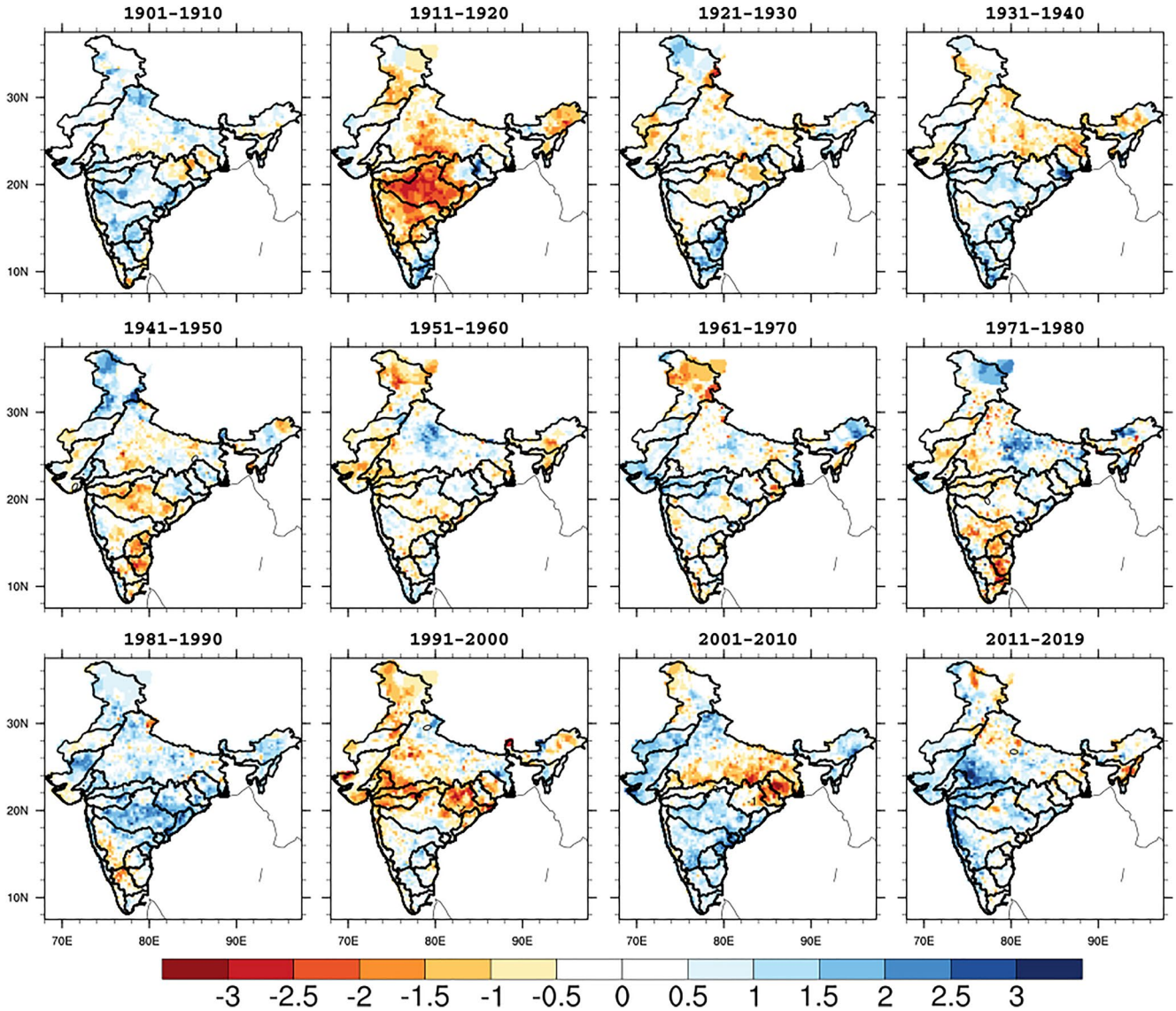

Figure 12. Decadal changes in average intensity of estimated standardized precipitation indices at a monthly time spanning over the Indian river basins.

(15%–58.74%) over the western ghats in west-flowing river basins of IRBs in the last 119 years. The findings of the study revealed a shift in extreme rainfall events over the western river basins of the central India homogeneous climate region. The findings in the context of IRBs can be used to frame hydrological hazard-centric policies and in formulating regional preparedness plans for national-scale mitigation and adaptation measures.

Conflict of Interest

The authors declare no conflicts of interest relevant to this study.

Data Availability Statement

The rainfall data is available online from IMD website (https://www.imdpune.gov.in/Clim_Pred_LRF_New/Grided_Data_Download.html). The SRTM datasets used in this study is available online from https://earthexplorer.usgs.gov/.

Acknowledgments
The authors are grateful to the DST-Mahamana Centre of Excellence in Climate Change Research, financially supported by the Department of Science and Technology, New Delhi under Climate Change Programme (DST/CCP/CoE/80/2017(G)). The authors are thankful to Earth Explorer for providing SRTM based Digital Elevation Model used in this study. The authors wish to thank the India Meteorological Department (IMD) for the observed gridded rainfall datasets.

References

Ali, H., Modi, P., & Mishra, V. (2019). Increased flood risk in Indian sub-continent under the warming climate. *Weather and Climate Extremes*, *25*(May). https://doi.org/10.1016/j.wace.2019.100212

Ayugi, B., Tan, G., Gnitou, G. T., Ojara, M., & Ongoma, V. (2020). Historical evaluations and simulations of precipitation over East Africa from Rossby centre regional climate model. *Atmospheric Research*, *232*(May 2019), 104705. https://doi.org/10.1016/j.atmosres.2019.104705

Bhalme, H. N., & Mooley, D. A. (1980). Large-scale droughts/floods and monsoon circulation. *Monthly Weather Review*, *108*(8), 1197–1211. https://doi.org/10.1175/1520-0493(1980)108<1197:LSDAMC>2.0.CO;2

Bhatia, U., & Ganguly, A. R. (2019). Precipitation extremes and depth-duration-frequency under internal climate variability. *Scientific Reports*, *9*(1), 9112. https://doi.org/10.1038/s41598-019-45673-3

Bishop, D. A., Williams, A. P., Seager, R., Fiore, A. M., Cook, B. I., Mankin, J. S., et al. (2019). Investigating the causes of increased twentieth-century fall precipitation over the Southeastern United States. *Journal of Climate*, *32*(2), 575–590. https://doi.org/10.1175/JCLI-D-18-0244.1

Bisht, D. S., Chatterjee, C., Raghuwanshi, N. S., & Sridhar, V. (2018). Spatio-temporal trends of rainfall across Indian river basins. *Theoretical and Applied Climatology*, *132*(1–2), 419–436. https://doi.org/10.1007/s00704-017-2095-8

Cai, W., Santoso, A., Wang, G., Weller, E., Wu, L., Ashok, K., et al. (2014). Increased frequency of extreme Indian ocean dipole events due to greenhouse warming. *Nature*, *510*(7504), 254–258. https://doi.org/10.1038/nature13327

Caporali, E., Lompi, M., Pacetti, T., Chiarello, V., & Fatichi, S. (2021). A review of studies on observed precipitation trends in Italy. *International Journal of Climatology*, *41*(S1), E1–E25. https://doi.org/10.1002/joc.6741

Carvalho, L. M. V. (2020). Assessing precipitation trends in the Americas with historical data: A review. *WIREs Climate Change*, *11*(2), 1–21. https://doi.org/10.1002/wcc.627

Charn, A. B., Collins, W. D., Parishani, H., Risser, M. D., & O'Brien, T. A. (2020). Microphysical sensitivity of superparameterized precipitation extremes in the contiguous United States due to feedbacks on large-scale circulation. *Earth and Space Science*, *7*, 1–16. https://doi.org/10.1029/2019EA000731

Chase, T. N., Knaff, J. A., Pielke, S. A., & Kalnay, E. (2003). Changes in global monsoon circulations since 1950. *Natural Hazards*, *29*(2), 229–254. https://doi.org/10.1023/A:1023638030885

Choudhury, A. D., & Krishnan, R. (2011). Dynamical response of the South Asian monsoon trough to latent heating from stratiform and convective precipitation. *Journal of the Atmospheric Sciences*, *68*(6), 1347–1363. https://doi.org/10.1175/2011JAS3705.1

Coles, S., Pericchi, L. R., & Sisson, S. (2003). A fully probabilistic approach to extreme rainfall modeling. *Journal of Hydrology*, *273*(1–4), 35–50. https://doi.org/10.1016/s0022-1694(02)00353-0

Coles, S. G. (2001). *An introduction to statistical modeling of extreme values*. Springer.

CWC. (2018). Reassessment of water availability in basins using spatial inputs. *BASIN PLANNING & MANAGEMENT ORGANISATION,CENTRAL WATER COMMISSION*. Retrieved from http://old.cwc.gov.in/main/downloads/ReassessmentMainReport.pdf

CWC. (2019). *WATER AND RELATED STATISTICS. Information system Organisation, water Planning & Project wing, central water Commission*. Retrieved from http://www.indiaenvironmentportal.org.in/files/file/water-and-related-statistics-2019.pdf

Dash, S. K., Kulkarni, M. A., Mohanty, U. C., & Prasad, K. (2009). Changes in the characteristics of rain events in India. *Journal of Geophysical Research: Atmospheres*, *114*(10), D10109. https://doi.org/10.1029/2008JD010572

Deshpande, N. R., Kothawale, D. R., & Kulkarni, A. (2016). Changes in climate extremes over major river basins of India. *International Journal of Climatology*, *36*(14), 4548–4559. https://doi.org/10.1002/joc.4651

Devanand, A., Huang, M., Ashfaq, M., Barik, B., & Ghosh, S. (2019). Choice of irrigation water management practice affects Indian summer monsoon rainfall and its extremes. *Geophysical Research Letters*, *46*(15), 9126–9135. https://doi.org/10.1029/2019GL083875

Donat, M. G., Lowry, A. L., Alexander, L. V., O'Gorman, P. A., & Maher, N. (2016). More extreme precipitation in the worldâ €TM s dry and wet regions. *Nature Climate Change*, *6*(5), 508–513. https://doi.org/10.1038/nclimate2941

EM-DAT. (2019). In *Centre for research on the Epidemiology of disasters (CRED) Publishes 2019 disaster Statistics*. Retrieved from https://www.un-spider.org/news-and-events/news/cred-publishes-2019-disaster-statisticshttps://cred.be/sites/default/files/adsr_2019.pdf

Ghosh, S., Das, D., Kao, S. C., & Ganguly, A. R. (2012). Lack of uniform trends but increasing spatial variability in observed Indian rainfall extremes. *Nature Climate Change*, *2*(2), 86–91. https://doi.org/10.1038/nclimate1327

Ghosh, S., Luniya, V., & Gupta, A. (2009). Trend analysis of Indian summer monsoon rainfall at different spatial scales. *Atmospheric Science Letters*, *10*(October), 285–290. https://doi.org/10.1002/asl.235

Goswami, B. N., Venugopal, V., Sangupta, D., Madhusoodanan, M. S., & Xavier, P. K. (2006). Increasing trend of extreme rain events over India in a warming environment. *Science*, *314*(5804), 1442–1445. https://doi.org/10.1126/science.1132027

Guhathakurta, P., & Rajeevan, M. (2008). Trends in the rainfall pattern over India. *International Journal of Climatology*, *28*, 1453–1469. https://doi.org/10.1002/joc.1640

Hänsel, S., Schucknecht, A., & Matschullat, J. (2016). The modified rainfall anomaly index (mRAI)—Is this an alternative to the Standardised Precipitation Index (SPI) in evaluating future extreme precipitation characteristics? *Theoretical and Applied Climatology*, *123*(3–4), 827–844. https://doi.org/10.1007/s00704-015-1389-y

Herold, N., Behrangi, A., & Alexander, L. V. (2017). Large uncertainties in observed daily precipitation extremes over land. *Journal of Geophysical Research*, *122*(2), 668–681. https://doi.org/10.1002/2016JD025842

Hodgkins, G. A., Dudley, R. W., Archfield, S. A., & Renard, B. (2019). Effects of climate, regulation, and urbanization on historical flood trends in the United States. *Journal of Hydrology*, *573*(August 2018), 697–709. https://doi.org/10.1016/j.jhydrol.2019.03.102

India-WRIS. (2012). *river basin atlas of India, RRSC-west, NRSC, ISRO*. Government of India Ministry of Water Resources.

IPCC. (2014). Summary for policymakers. In C. B.Field, V. R.Barros, D. J.Dokken, K. J.Mach, M. D.Mastrandrea, T. E.Bilir, et al. (Eds.), *Climate change 2014: Impacts, Adaptation, and Vulnerability. Part A: Global and Sectoral aspects. Contribution of Working Group II to the Fifth Assessment Report of the Intergovernmental Panel on Climate Change*. Cambridge University Press. (pp. 1–32).

Joshi, U. R., & Rajeevan, M. (2006). *Trends in precipitation extremes over India*. National Climate Centre, India Meteorological Department.

Kao, S. C., & Ganguly, A. R. (2011). Intensity, duration, and frequency of precipitation extremes under 21st-century warming scenarios. *Journal of Geophysical Research: Atmospheres*, *116*(16), 1–14. https://doi.org/10.1029/2010JD015529

Kendall, M. G. (1948). *Rank correlation methods* (4th ed.). Charles Griffin.

Khan, S., Kuhn, G., Ganguly, A. R., Erickson, D. J., & Ostrouchov, G. (2007). Spatio-temporal variability of daily and weekly precipitation extremes in South America. *Water Resources Research*, *43*, 1–25. https://doi.org/10.1029/2006WR005384

Krishnamurthy, C. K. B., Lall, U., & Kwon, H. H. (2009). Changing frequency and intensity of rainfall extremes over India from 1951 to 2003. *Journal of Climate*, *22*(18), 4737–4746. https://doi.org/10.1175/2009JCLI2896.1

Kunkel, K. E., Easterling, D. R., Redmond, K., & Hubbard, K. (2003). Temporal variations of extreme precipitation events in the United States: 1895-2000. *Geophysical Research Letters*, *30*(17), 1–4. https://doi.org/10.1029/2003GL018052

Libertino, A., Ganora, D., & Claps, P. (2019). Evidence for increasing rainfall extremes remains elusive at large spatial scales: The case of Italy. *Geophysical Research Letters*, *46*(13), 7437–7446. https://doi.org/10.1029/2019GL083371

Lu, M., Xu, Y., Shan, N., Wang, Q., Yuan, J., & Wang, J. (2019). Effect of urbanisation on extreme precipitation based on nonstationary models in the Yangtze River Delta metropolitan region. The *Science of the Total Environment*, *673*, 64–73. https://doi.org/10.1016/j.scitotenv.2019.03.413

Mall, R. K., Gupta, A., Singh, R., Singh, R. S., & Rathore, L. S. (2006). Water resources and climate change: An Indian perspective. *Current Science*, *90*(12), 1610–1626. Retrieved from http://www.jstor.org/stable/24091910

Mall, R. K., Srivastava, R. K., Banerjee, T., Mishra, O. P., Bhatt, D., & Sonkar, G. (2019). Disaster risk reduction including climate change adaptation over South Asia: Challenges and ways forward. *International Journal of Disaster Risk Science*, *10*(1), 14–27. https://doi.org/10.1007/s13753-018-0210-9

Mann, H. B. (1945). Nonparametric tests against trend. *Econometrica*, *13*, 245–259. https://doi.org/10.2307/1907187

Mannshardt-Shamseldin, E. C., Smith, R. L., Sain, S. R., Mearns, L. O., & Cooley, D. (2012). Downscaling extremes: A comparison of extreme value distributions in point-source and gridded precipitation data. *Annals of Applied Statistics*, *6*, 484–502. https://doi.org/10.1214/09-AOAS287

Martins, E. S., & Stedinger, J. R. (2000). Generalized maximum-likelihood generalized extreme-value quantile estimators for hydrologic data. *Water Resources Research*, *36*, 737–744. https://doi.org/10.1029/1999WR900330

McKee, T. (1993). The relationship of drought frequency and duration to time scales. *Proceedings of the 8th Conference on Applied Climatology*, *17*(22), 179–183.

Met Glossary. Meteorological Terminology and Glossary published by IMD, Pun. Retrieved from https://www.imdpune.gov.in/Weather/Reports/glossary.pdf

Mohanty, A. (2020). *Preparing India for extreme climate events, (December)* (p. 68). Retrieved from https://www.ceew.in/publications/preparing-india-extreme-climate-events

Narayanan, P., Basistha, A., & Sachdeva, K. (2016). Understanding trends and shifts in rainfall in parts of northwestern India based on global climatic indices. *Weather*, *71*(8), 198–203. https://doi.org/10.1002/wea.2746

Ogega, O. M., Koske, J., Kung'u, J. B., Scoccimarro, E., Endris, H. S., & Mistry, M. N. (2020). Heavy precipitation events over east Africa in a changing climate: Results from CORDEX RCMs. *Climate Dynamics*, *55*(3–4), 993–1009. https://doi.org/10.1007/s00382-020-05309-z

Pai, D. S., Sridhar, L., Badwaik, M. R., & Rajeevan, M. (2015). Analysis of the daily rainfall events over India using a new long period (1901–2010) high resolution (0.25° × 0.25°) gridded rainfall data set. *Climate Dynamics*, *45*(3–4), 755–776. https://doi.org/10.1007/s00382-014-2307-1

Pai, D. S., Sridhar, L., Rajeevan, M., Sreejith, O. P., Satbhai, N. S., & Mukhopadhyay, B. (2014). Development of a new high spatial resolution (0.25° × 0.25°) long period (1901-2010) daily gridded rainfall data set over India and its comparison with existing data sets over the region. *Mausam*, *65*(1), 1–18.

Papalexiou, S. M., & Montanari, A. (2019). Global and regional increase of precipitation extremes under global warming. *Water Resources Research*, *55*(6), 4901–4914. https://doi.org/10.1029/2018WR024067

Raj, E. E., Kumar, R. R., & Ramesh, K. V. (2020). El niño–southern oscillation (ENSO) impact on tea production and rainfall in south India. *Journal of Applied Meteorology and Climatology*, *59*(4), 651–664. https://doi.org/10.1175/JAMC-D-19-0065.1

Rajeevan, M., Bhate, J., & Jaswal, A. K. (2008). Analysis of variability and trends of extreme rainfall events over India using 104 years of gridded daily rainfall data. *Geophysical Research Letters*, *35*(18), 1–6. https://doi.org/10.1029/2008GL035143

Rajeevan, M., Bhate, J., Rajeevan, M., Bhate, J., Kale, J. D., & Lal, B. (2006). High resolution daily gridded rainfall data for the Indian region: Analysis of break and active. *Current Science*, *91*(3), 296–306. Retrieved from https://www.jstor.org/stable/24094135

Ratna, S. B., Cherchi, A., Osborn, T. J., Joshi, M., & Uppara, U. (2021). The extreme positive Indian Ocean Dipole of 2019 and associated Indian summer monsoon rainfall response. *Geophysical Research Letters*, *48*(2), 1–11. https://doi.org/10.1029/2020GL091497

Rooy, V. (1965). A rainfall anomaly index (RAI) independent of time and space. *Notos* (14), 43–48.

Roxy, M. K., Ghosh, S., Pathak, A., Athulya, R., Mujumdar, M., Murtugudde, R., et al. (2017). A threefold rise in widespread extreme rain events over central India. *Nature Communications*, *8*(1), 1–11. https://doi.org/10.1038/s41467-017-00744-9

Roy, S. S., & Balling, R. C. (2004). Trends in extreme daily precipitation indices in India. *International Journal of Climatology*, *24*(4), 457–466. https://doi.org/10.1002/joc.995

Saha, M., Mitra, P., & Nanjundiah, R. S. (2017). Deep learning for predicting the monsoon over the homogeneous regions of India. *Journal of Earth System Science*, *126*, 54. https://doi.org/10.1007/s12040-017-0838-7

Sanderson, B. M., Wobus, C., Mills, D., Zarakas, C., Crimmins, A., Sarofim, M. C., & Weaver, C. (2019). Informing future risks of Record-level rainfall in the United States. *Geophysical Research Letters*, *46*(7), 3963–3972. https://doi.org/10.1029/2019GL082362

Santos, M., Fonseca, A., Fragoso, M., & Santos, J. A. (2019). Recent and future changes of precipitation extremes in mainland Portugal. *Theoretical and Applied Climatology*, *137*(1–2), 1305–1319. https://doi.org/10.1007/s00704-018-2667-2

Shah, D., & Mishra, V. (2021). Strong influence of changes in terrestrial water storage on flood potential in India. *Journal of Geophysical Research: Atmospheres*, *126*(1), e2020JD033566. https://doi.org/10.1029/2020JD033566

Singh, O., Khan, T. M. A., & Rahman, M. S. (2001). Has the frequency of intense tropical cyclones increased in the north Indian Ocean? *Current Science*, 575–580.

Suman, M., & Maity, R. (2020). Southward shift of precipitation extremes over south Asia: Evidences from CORDEX data. *Scientific Reports*, *10*(1), 6452. https://doi.org/10.1038/s41598-020-63571-x

Tabari, H. (2020). Climate change impact on flood and extreme precipitation increases with water availability. *Scientific Reports*, *10*, 1–10. https://doi.org/10.1038/s41598-020-70816-2

Tegegne, G., & Melesse, A. M. (2020). Multimodel ensemble projection of hydro-climatic extremes for climate change impact assessment on water resources. *Water Resources Management*, *34*(9), 3019–3035. https://doi.org/10.1007/s11269-020-02601-9

Tegegne, G., Melesse, A. M., & Alamirew, T. (2021). Projected changes in extreme precipitation indices from CORDEX simulations over Ethiopia, East Africa. *Atmospheric Research*, *247*, 105156. https://doi.org/10.1016/j.atmosres.2020.105156

Tong, S., Li, X., Zhang, J., Bao, Y., Bao, Y., Na, L., & Si, A. (2019). Spatial and temporal variability in extreme temperature and precipitation events in Inner Mongolia (China) during 1960–2017. The *Science of the Total Environment*, *649*, 75–89. https://doi.org/10.1016/j.scitotenv.2018.08.262

Trenberth, K. E., Dai, A., vander Schrier, G., Jones, P. D., Barichivich, J., Briffa, K. R., & Sheffield, J. (2014). Global warming and changes in drought. *Nature Climate Change*, *4*(1), 17–22. https://doi.org/10.1038/nclimate2067

Turner, A. G., & Annamalai, H. (2012). Climate change and the South Asian summer monsoon. *Nature Climate Change*, *2*(8), 587–595. https://doi.org/10.1038/nclimate1495

Van De Vyver, H. (2012). Spatial regression models for extreme precipitation in Belgium. *Water Resources Research*, *48*, 1–17. https://doi.org/10.1029/2011WR011707

Zhang, X., Alexander, L., Hegerl, G. C., Jones, P., Tank, A. K., Peterson, T. C., et al. (2011). Indices for monitoring changes in extremes based on daily temperature and precipitation data. *WIREs Climate Change*, *2*(6), 851–870. https://doi.org/10.1002/wcc.147